

NAVAL POSTGRADUATE SCHOOL Monterey, California



THESIS

PARAMETERIZING SURFACE FLUXES IN THE ARCTIC

by

Anna C. Bryant

September 2001

Thesis Advisor:
Second Reader:

Peter Guest
Qing Wang

Approved for public release; distribution is unlimited.

Report Documentation Page

Report Date 30 Sep 2001	Report Type N/A	Dates Covered (from... to) -
Title and Subtitle Parameterizing Surface Fluxes in the Arctic	Contract Number	
	Grant Number	
	Program Element Number	
Author(s) Name Anna C. Bryant	Project Number	
	Task Number	
	Work Unit Number	
Performing Organization Name(s) and Address(es) Research Office Naval Postgraduate School Monterey, Ca 93943-5138	Performing Organization Report Number	
Sponsoring/Monitoring Agency Name(s) and Address(es)	Sponsor/Monitor's Acronym(s)	
	Sponsor/Monitor's Report Number(s)	
Distribution/Availability Statement Approved for public release, distribution unlimited		
Supplementary Notes		
Abstract		
Subject Terms		
Report Classification unclassified	Classification of this page unclassified	
Classification of Abstract unclassified	Limitation of Abstract UU	
Number of Pages 80		

REPORT DOCUMENTATION PAGE

Form Approved OMB No. 0704-0188

Public reporting burden for this collection of information is estimated to average 1 hour per response, including the time for reviewing instruction, searching existing data sources, gathering and maintaining the data needed, and completing and reviewing the collection of information. Send comments regarding this burden estimate or any other aspect of this collection of information, including suggestions for reducing this burden, to Washington headquarters Services, Directorate for Information Operations and Reports, 1215 Jefferson Davis Highway, Suite 1204, Arlington, VA 22202-4302, and to the Office of Management and Budget, Paperwork Reduction Project (0704-0188) Washington DC 20503.

1. AGENCY USE ONLY (Leave blank)		2. REPORT DATE September 2001	3. REPORT TYPE AND DATES COVERED Master's Thesis	
4. TITLE AND SUBTITLE Title Parameterizing Surface Fluxes in the Arctic			5. FUNDING NUMBERS	
6. AUTHOR (S) Name Anna C. Bryant			8. PERFORMING ORGANIZATION REPORT NUMBER	
7. PERFORMING ORGANIZATION NAME(S) AND ADDRESS(ES) Naval Postgraduate School Monterey, CA 93943-5000			10. SPONSORING/MONITORING AGENCY REPORT NUMBER	
9. SPONSORING / MONITORING AGENCY NAME(S) AND ADDRESS(ES)			11. SUPPLEMENTARY NOTES The views expressed in this thesis are those of the author and do not reflect the official policy or position of the U.S. Department of Defense or the U.S. Government.	
12a. DISTRIBUTION / AVAILABILITY STATEMENT Approved for public release; distribution is unlimited			12b. DISTRIBUTION CODE	
13. ABSTRACT (maximum 200 words) <p>There is a need for computationally efficient methods to determine surface radiation in the Arctic based on surface parameters such as cloud presence, sun angle, temperature and other easily measured variables.</p> <p>This study uses data from the SHEBA project to verify simple radiation parameterizations and to compare with other locations. Skies during SHEBA were usually either totally clear or totally overcast, with low clouds predominating, especially in the non-winter seasons. This resulted in large changes in radiation every time the cloud coverage changed.</p> <p>There was a large range in the skill of the parametric equations. The most accurate equations had average total errors of 9 Wm^{-2}, 14 Wm^{-2}, 22 Wm^{-2} and 59 Wm^{-2} for downwelling longwave in clear skies, cloudy skies, shortwave clear and cloudy skies respectively. Compared to the Weddell Sea (Antarctic) the average downward longwave radiation was greater for all sky conditions. Shortwave values were comparable to the Weddell Sea, although there was large variability.</p>				
14. SUBJECT TERMS Meteorology Arctic Surface Flux Longwave Radiation Shortwave Radiation			15. NUMBER OF PAGES 80	
17. SECURITY CLASSIFICATION OF REPORT Unclassified	18. SECURITY CLASSIFICATION OF THIS PAGE Unclassified	19. SECURITY CLASSIFICATION OF ABSTRACT Unclassified	16. PRICE CODE 20. LIMITATION OF ABSTRACT UL	

NSN 7540-01-280-5500

Standard Form 298 (Rev. 2-89)
Prescribed by ANSI Std. Z39-18

THIS PAGE INTENTIONALLY LEFT BLANK

Approved for public release; distribution is unlimited

PARAMETERIZING SURFACE FLUXES IN THE ARCTIC

Anna C. Bryant
Lieutenant, United States Navy
B.S., University of South Carolina, 1996

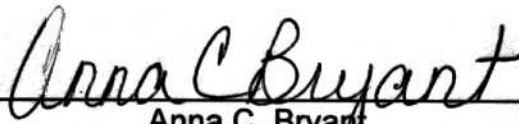
Submitted in partial fulfillment of the
requirements for the degree of

MASTER OF SCIENCE IN METEOROLOGY AND
PHYSICAL OCEANOGRAPHY

from the

NAVAL POSTGRADUATE SCHOOL
SEPTEMBER 2001

Author:



Anna C. Bryant

Approved by:



Peter S. Guest, Thesis Advisor



Qing Wang, Second Reader



Carlyle H. Wash, Chairman
Department of Meteorology

THIS PAGE INTENTIONALLY LEFT BLANK

ABSTRACT

There is a need for computationally efficient methods to determine surface radiation in the Arctic based on surface parameters such as cloud presence, sun angle, temperature and other easily measured variables.

This study uses data from the SHEBA project to verify simple radiation parameterizations and to compare with other locations. Skies during SHEBA were usually either totally clear or totally overcast, with low clouds predominating, especially in the non-winter seasons. This resulted in large changes in radiation every time the cloud coverage changed.

There was a large range in the skill of the parametric equations. The most accurate equations had average total errors of 9 Wm^{-2} , 14 Wm^{-2} , 22 Wm^{-2} and 59 Wm^{-2} for downwelling longwave in clear skies, cloudy skies, shortwave clear and cloudy skies respectively. Compared to the Weddell Sea (Antarctic) the average downward longwave radiation was greater for all sky conditions. Shortwave values were comparable to the Weddell Sea, although there was large variability.

THIS PAGE INTENTIONALLY LEFT BLANK

TABLE OF CONTENTS

I. INTRODUCTION	1
II. MEASUREMENT AND DATA ORGANIZATION.....	3
A. CLOUD MEASUREMENTS	3
B. LONGWAVE RADIATION.....	4
C. SHORTWAVE RADIATION	6
D. METEOROLOGICAL VARIABLES.....	6
III. RESULTS AND DISCUSSION	9
A. CLOUDS	9
B. LONGWAVE RADIATION.....	19
1. Clear Sky Downwelling Longwave Radiation.....	24
2. Overcast Sky Longwave Downwelling Radiation	27
3. Partly Cloudy Sky Longwave Downwelling Radiation	31
C. SHORTWAVE RADIATION	34
1. Clear Sky Downwelling Shortwave Radiation	36
2. Overcast Sky Shortwave Downwelling Radiation.....	39
3. Partly Cloudy Sky Shortwave Downwelling Radiation.....	42
IV. CONCLUSIONS	45
APPENDIX A. GRAPHS OF TESTED EQUATIONS	49
LIST OF REFERENCES.....	63
INITIAL DISTRIBUTION LIST	65

THIS PAGE INTENTIONALLY LEFT BLANK

LIST OF FIGURES

Figure 1. SHEBA drift camp path. Taken from SHEBA web site.....	2
Figure 2. Eppley Precision Infrared Radiometers (PIR) and Eppley Precision Solar Radiometers (PSP) measuring the upward and downward longwave and shortwave radiation at the SHEBA drift camp.	5
Figure 3. Meteorological tower at the SHEBA drift camp.	7
Figure 4. Cloud coverage in tenths for entire SHEBA data collection period of 11 months indicating number of occurrences for each reading.	10
Figure 5. Cloud coverage by seasons. Counts indicate the number of readings in each tenths category.	11
Figure 6. Cloud coverage by month depicting number of occurrences for each cloud coverage level in tenths.	13
Figure 7. Cloud coverage by month depicting number of occurrences for each cloud coverage level in tenths.	13
Figure 8. Cloud coverage by month depicting number of occurrences for each cloud coverage level in tenths.	14
Figure 9. Histogram of cloud coverage for all cloud heights by month and tenths for entire SHEBA measurement period.	14
Figure 10. Cloud coverage by month for entire SHEBA measurement cycle, depicting number of cloud measurements taken and those that were low clouds (cloud base height less than 5000 feet or 1524 meters).	15
Figure 11. Percent of low cloud coverage in non-clear conditions (defined as cloud coverage greater than 0).	16
Figure 12. Histogram of the number of occurrences of clouds by cloud height.	18
Figure 13. From Makshtas et al., (1998), depicting area of study. Limits of study are bounded by dashed line. SHEBA study area, shown in Figure 1., was in much the same area.....	19
Figure 14. Time series of the net measured radiation flux (W/m ²). January 1, 1998 is given the Julian date of 366.	22
Figure 15. Net longwave radiation flux by cloudiness level. Net flux is calculated by longwave upward-downward. Partly cloudy skies have cloudiness percentages >0% and <100%.	22
Figure 16. Surface temperature expressed as blackbody radiation (σT_{air}^4) vs. measured longwave radiation for completely clear skies, completely overcast skies and partly cloudy skies.	23
Figure 17. Measured and parameterized LW↓ from the three most accurate parametric equations during completely clear skies with 1159 hourly points.	26
Figure 18. Time series showing the predicted LW↓ and the measured LW↓ for the three best performing parametric equations.....	27
Figure 19. Most accurate parametric equations for LW↓ during completely overcast skies with 4026 hourly points.	29
Figure 20. Time series of the four best parametric formulas under overcast conditions. Each graph has the predicted LW↓ (red +) and the measured LW↓ (blue *) for each hourly measurement.	30
Figure 21. Scatter plot of error for three best prediction equations for LW↓ under partly cloudy sky conditions.....	33

Figure 22. Time series of predicted and measured LW↓ for the three best prediction equations under partly cloudy skies.....	33
Figure 23. Scatter plot of the angle of the sun above the horizon and measured downward shortwave radiation.....	35
Figure 24. Time series of the measured SW↓ (W/m2) by sky condition.	36
Figure 25. Scatter error plots for the three best parametric formulas under clear skies. Error is calculated from predicted SW↓ - measured SW↓.....	38
Figure 26. Time series of predicted (blue *) and measured (red +) for the three best parametric formulas under clear skies.....	39
Figure 27. Scatter error plots for best parametric equation and a best fit (linear) for shortwave downward radiation under overcast skies.....	41
Figure 28. Time series of downward shortwave for the best parametric equation and a linear best fit to the data under overcast skies.	42

LIST OF TABLES

Table 1. Cloud coverage for the four season during the entire SHEBA measurement period.....	12
Table 2. Cloud coverage in count and percent for low clouds. Each count is one reading of cloud base height by ceilometer or LIDAR for that month. Total count is the number of total readings, regardless of amount of coverage.....	17
Table 3. Various parameterizations for clear sky downwelling longwave radiation.	24
Table 4. Mean Error, Standard Deviation and Total Error between measured longwave radiation and parametric equations for completely clear skies. Bold indicates the best three formulas. Negative values indicate predicted values were less than measured values.	25
Table 5. Parametric equations tested for overcast skies.	28
Table 6. Mean Error, Standard Deviation and Total Error between measured longwave radiation and parametric equations for occurrences of completely overcast skies. Bold indicates the best four parametric formulas.	28
Table 7. Parametric equations for partly cloudy skies.	32
Table 8. Mean Error, Standard Deviation and Total Error between measured longwave radiation and parametric equations for occurrences of partly cloudy skies. The three best of the formulas are in bold.	32
Table 9. Parametric equations for shortwave radiation under clear skies.	37
Table 10. Mean Error, Standard Deviation and Total Error between measured longwave radiation and parametric equations for occurrences of clear skies. The three best formulas are in bold.....	37
Table 11. Parametric equations for shortwave downward radiation under overcast skies.	40
Table 12. Downward shortwave parametric equation error statistics. Bold indicates best performers.	40
Table 13. Parametric equations for shortwave radiation under partly cloudy skies.	43
Table 14. Error statistics for parametric shortwave downward radiation equations under partly cloudy skies and a quadratic best fit to the data.	43

THIS PAGE INTENTIONALLY LEFT BLANK

ACKNOWLEDGEMENTS

The author would like to acknowledge the support of the SHEBA Surface Atmospheric Flux Group (ASFG), including Edgar L. Andreas, Christopher W. Fairall, Peter S. Guest and P. Ola G. Persson, for providing the data used in this thesis. Their work was supported by the National Science Foundation Office of Polar Programs, in particular grant OPP-9701390.

The author would like to thank Qing Wang for her performance as second reader and the many helpful suggestions she offered.

The author would like to make special acknowledgement to Christopher W. Fairall of the ASFG and colleagues at Environmental Technical Laboratory for providing the cloud data used in this thesis.

THIS PAGE INTENTIONALLY LEFT BLANK

I. INTRODUCTION

Polar regions are expected to have an amplified response to global warming. However, many of the important processes in polar regions are poorly understood, including the effects of clouds on surface radiation. There is a need to develop and verify computationally efficient radiation parameterizations for polar regions. Several such parameterizations have been published but the amount of testing on these parameterizations varies.

Because of their simplicity, computationally efficient parameterizations are not expected to perform as well as multi-level radiation models. These relatively simple equations utilize a minimum of measured variables, such as temperature near the surface, relative humidity, relative humidity with respect to ice, and vapor pressure in order to predict the downward radiation. Some require only the input of temperature (longwave), sun angle (shortwave), and cloud fraction (all radiation). Despite the creation of increasingly complex models, there is still a need for these simple equations. They can be used by researchers with limited computing access, in desktop models and incorporated in the newer high-level models.

The parameterizations are based, in many cases, on limited data sets, often from a single location. Early equations were developed with equipment now antiquated and others were developed only for specific applications. Many have never been tested with data sets of recent origin or covering long time periods.

To investigate the quality, accuracy and ease of use of a wide variety of previously published parameterizations, a large Arctic data set of recent acquisition was needed. During the time period between October 1997 and October 1998, the Surface Heat Budget of the Arctic Ocean Experiment (SHEBA), established a drift camp in the Beaufort Sea where an extensive array of meteorological measurements were taken (Figure 1) (Persson et al., 2001).

These measurements created the data set used in this investigation of parametric equations for longwave and shortwave downward radiation.

Equations formulated for use specifically in the Antarctic were also compared with this Arctic data set to estimate their suitability for the Arctic and to compare Arctic vs. Antarctic radiation characteristics.

The primary focus of the investigation was to perform an evaluation of parametric equations, however a summary of net radiation is also of value here. Since clouds affect the longwave and shortwave radiation to such a high degree, a survey of the cloud coverage for the SHEBA drift camp is compared with another recent study (Makshtas et al., 1998).

Results of this investigation would be of use to those formulating new models and improving the accuracy of existing ones by incorporating the best of the parametric equations. The cloud fraction and height data, added to the existing modern body of work, provides an additional source for characterizing the climate of the Arctic.

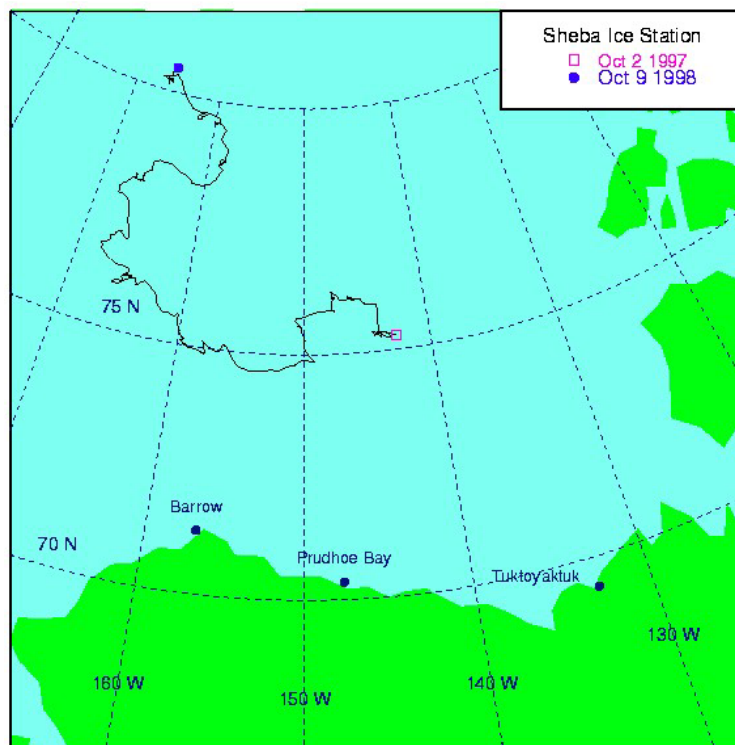


Figure 1. SHEBA drift camp path. Taken from SHEBA web site.

II. MEASUREMENT AND DATA ORGANIZATION

Data were collected during the SHEBA project over a period covering slightly more than eleven months. SHEBA's drift camp and site included individual sites and measurements taken by various groups participating in the project, each of which is named with their measurements in the following chapter.

All data used in this paper were pre-screened for quality by members of the SHEBA Atmospheric Surface Flux Group (ASFG) and Environmental Technology Laboratory (ETL). Many instruments and their measurements were redundant and comparison between them assisted in the quality control as well as standard calibrations and instrument maintenance.

The dates of the experiment overlapped two calendar years. To facilitate ease of handling the data, Julian dates after December 31, 1997 were added to day 365 for the year 1997. The final date of measurement is 638.9167, which equates to Julian date 273.9167 of 1998. All graphs reflect this extended Julian date system.

A. CLOUD MEASUREMENTS

Continuous measurements of cloud-base height and the presence of cloud above the sensors were taken during the SHEBA measurement phase. Measurements were taken with both LIDAR and a laser ceilometer. This data set was compiled using a LIDAR at the Atmospheric Radiation Measurement (ARM) site, which was on the SHEBA vessel, until it permanently malfunctioned in August of 1998 (C. Fairall, pers. com.). After August, ceilometer measurements taken at the NOAA ETL site, also on the SHEBA ship, were used.

All data were averaged into hourly measurements using the following method. Cloud fraction was obtained by dividing the total number of readings in an hour in which cloudiness was detected by the total number of measurements in an hour. Cloud-base height is an average of all cloud-base heights registered during the course of an hour.

In total, there were 7,452 individual hours of measurement. Of that number, 121 readings were unusable leaving 7,331 useful measurements. All 7,331 measurements were used for quantifying cloud base height and cloud fraction, although significantly fewer measurements in this data set were used to study the longwave and shortwave radiation properties. The lower number of measurements included in those sections are due to editing processes with those data as explained in the corresponding sections.

B. LONGWAVE RADIATION

Longwave radiation measurements were taken with Eppley Precision Infrared Radiometer (PIR) hemispheric flux pyrgeometers in both the upward and downward directions (Figure 2). The sampling interval was 5 seconds with a final measurement provided by averaging the data for one-hour intervals (Persson et al., 2001).

Discussion regarding the specifics of equipment maintenance, topographical changes and anomalous weather or shadowing is given in Persson et al. (2001). The radiometers at the ASFG site were placed at a height of 1.5-2.0 meters above the snow surface. Longwave radiometers were affixed to a mast located approximately 25 meters horizontally from the 20-meter high meteorological tower (Persson et al., 2001).

During the month of July 1998, a melt pond formed within the view area for the downward facing radiometers, which remained until late August. A time coincident malfunction in the sensor at this time caused several days of missing data during this period.

The nearby meteorological tower also cast a shadow in low sun angles. This shadow appeared during the local mid-morning periods in winter (approximately 1800-1900 UTC). By installing fans and maintaining a frequent cleaning cycle, the radiometers experienced nearly ice-free conditions throughout the measurement cycle. (Persson et al., 2001).

After averaging, there were 8,114 hourly measurements of longwave radiation. Due to missing measurements in the cloud data set, specifically the 2300 UTC measurement for each day, and days in which there were equipment

malfunctions, the longwave radiation data set was edited to eliminate measurement periods not included in the cloud data set.

Some longwave radiation measurements were eliminated due to questionable measurements during periods of icing or missing measurements due to power losses. A secondary editing process took place that eliminated any radiation measurement in one direction in which the opposing direction measurement for that period was missing. For example, if the downward was missing due to icing, then the upward was eliminated for that time period as well.

A final editing process eliminated hourly measurements in which a meteorological variable required for the parametric equations or the shortwave measurement was missing, also due to power losses or equipment failure. After this editing process there remained 5,927 hourly measurements of upward and downward longwave radiation.

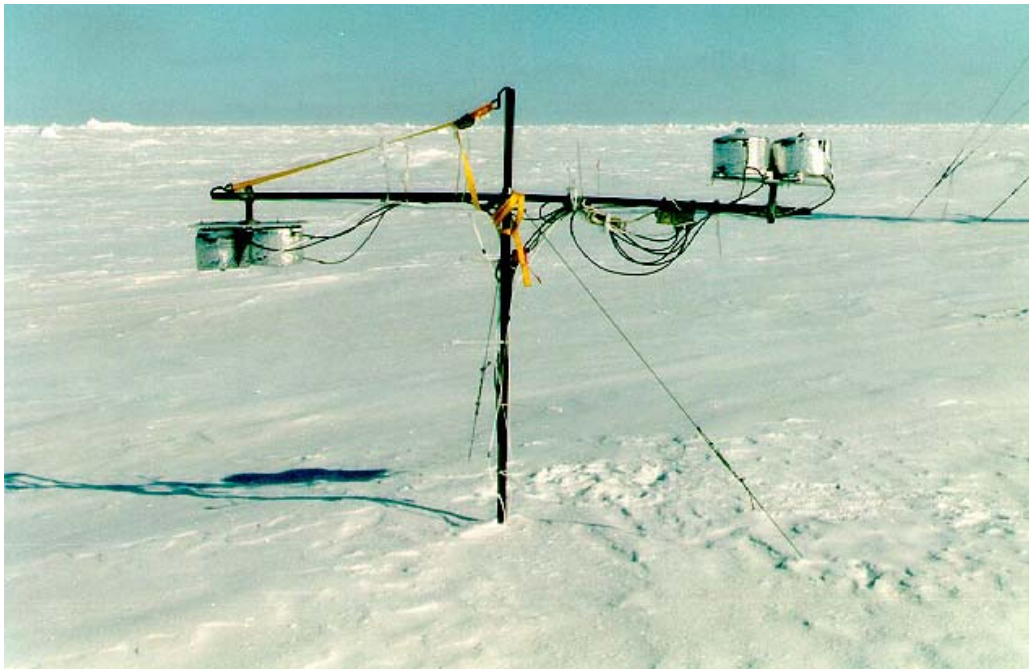


Figure 2. Eppley Precision Infrared Radiometers (PIR) and Eppley Precision Solar Radiometers (PSP) measuring the upward and downward longwave and shortwave radiation at the SHEBA drift camp.

C. SHORTWAVE RADIATION

Shortwave radiation in both the upward and downward directions was measured with Eppley Precision Solar pyranometers (PSP) at a 5 second sampling interval (Persson et al., 2001). Each sensor was located 1.5-2.0 meters above the surface of the snow (Figure 2). Averaging to a period of one hour was also done to achieve a final set of 8,114 measurements.

Further editing was done in the same manner as described for the longwave measurements, leaving a data set consisting of 5,927 measurements, each representing one hour for an eleven month period.

D. METEOROLOGICAL VARIABLES

All of the parametric equations for longwave radiation used in this study required an air temperature input close to the surface. Some equations also required variables such as relative humidity, RH, relative humidity with respect to ice, RH_i, vapor pressure, e , or variables needed to calculate e , pressure, p , and absolute humidity, q .

Equipment mounted on a 20-meter meteorological tower near the radiometer site collected all the required variables at five levels (figure 3). The lowest level of tower measurements was used for this study to be consistent with previous measurements that the tested parameterizations were developed from. Usually there was little variation in the temperature at different levels.

The exact height of the instruments above the snow surface varied in accordance with the snow depth, however the height varied between 1.9-3.0 meters with an average height of 2.2 meters (Persson et al., 2001).

The difference between temperature at the surface (T_{sfc}) and at the lowest level of the tower (T1) averaged only 0.51 °C in absolute value, with T1 being the higher of the two. This is important because remote sensing of surface temperature allows for wider use of these parametric equations. The small difference between the two measurements on an average basis means that remotely sensed surface temperatures would not strongly affect the skill level of these parametric equations. The editing process was the same as that for the longwave and shortwave radiation measurements.

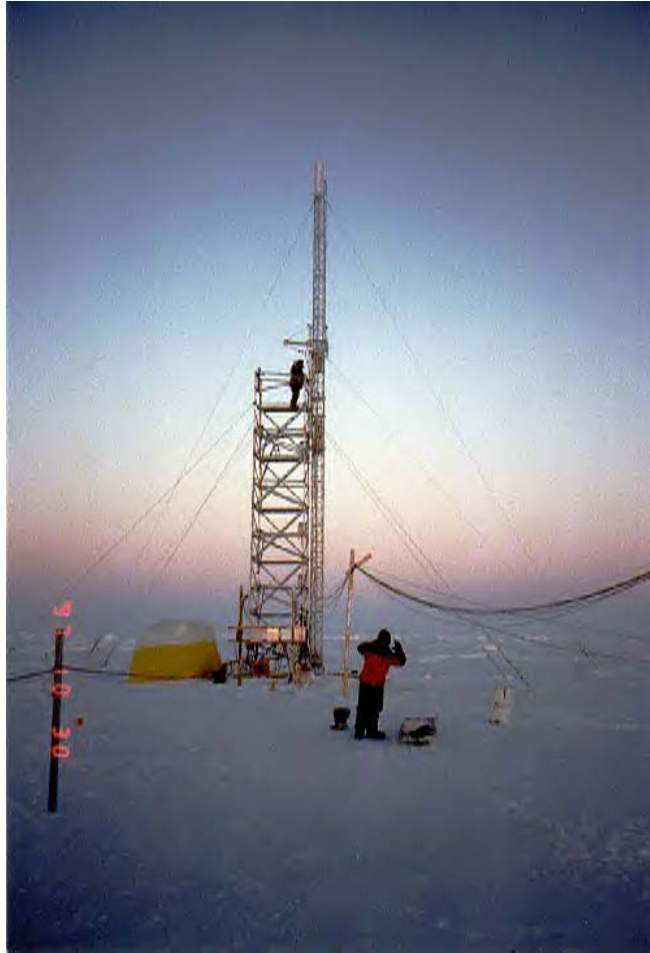


Figure 3. Meteorological tower at the SHEBA drift camp.

THIS PAGE INTENTIONALLY LEFT BLANK

III. RESULTS AND DISCUSSION

A. CLOUDS

The performance of any thermodynamic sea ice or polar atmosphere model depends upon the ability to accurately depict the clouds in the same region. The presence of clouds, their heights, thicknesses and types all significantly affect the radiation balance

There is a strong relationship between the presence of clouds and the amount of downward longwave and shortwave radiation reaching the surface. Clouds scatter and absorb shortwave radiation, causing less to reach the surface. Longwave radiation in the downward direction is enhanced by the presence of clouds, which are effective infrared radiators. Therefore, the evolution of clouds in the area of the SHEBA measurement site is crucial for understanding radiative properties.

Areal coverage, height, ice/liquid water content and a number of other cloud-related variables also affect surface radiation (Curry and Ebert, 1990). This brings up some of the limitations inherent to the SHEBA data set. Cloud measurements were taken from a single site in the drift camp, so the areal coverage was limited to the region of drift. Only cloud base height is available and there is no coinciding data set that provides thickness measurements for the clouds. Hence, the simple parameterizations examined in this study cannot be expected to account for all the variations in radiation that were observed during SHEBA, but only characterize them in a limited manner.

The U-shaped distribution of clouds for the entire 11-month SHEBA measurement period (Figure 4), mirrors the results found by other investigators (e.g. Makshtas et al., 1998). Although the SHEBA period is just shy of an entire year, it is clear that cloud coverage mainly falls in the 0-2 tenths and 8-10 tenths categories, similar to the known climatology.

Figure 5 compares results from different seasons. It illustrates that in spring, summer and fall the U-shaped distribution is lopsided with most cases having high coverage. In winter, however, there are more clear cases, making the U-shape more symmetric. During this season there are more instances of clear skies with less than 2 tenths cloud coverage than overcast skies with greater than 8 tenths of coverage by a small margin, resulting in a nearly equal U-shaped distribution. This is in obvious contrast to the other seasons where overcast skies dominate.

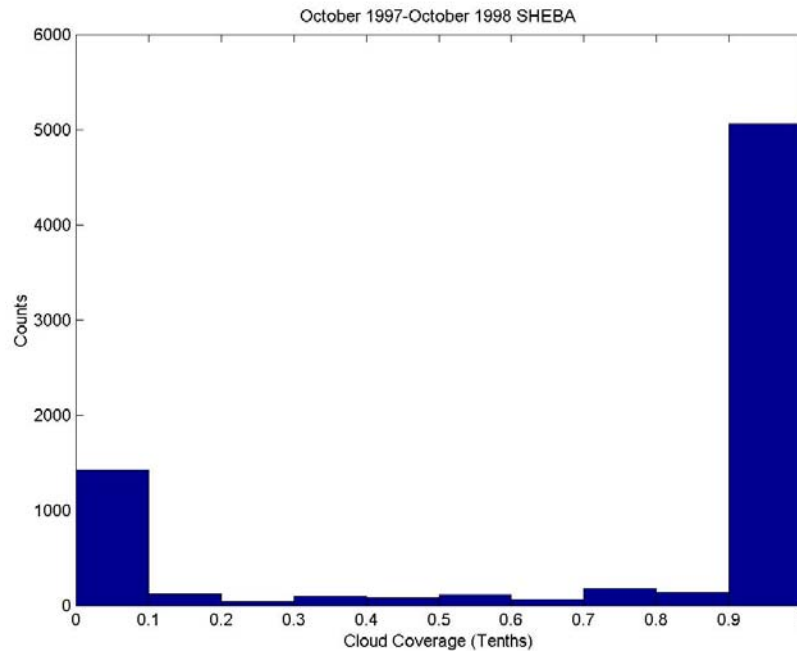


Figure 4. Cloud coverage in tenths for entire SHEBA data collection period of 11 months indicating number of occurrences for each reading.

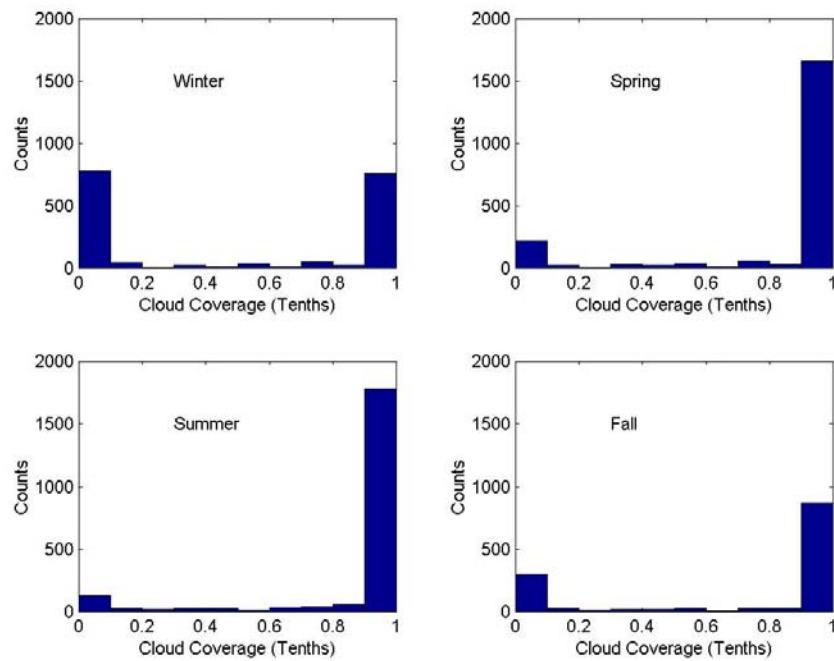


Figure 5. Cloud coverage by seasons. Counts indicate the number of readings in each tenths category.

The numerical breakdown of these graphs (Table 1) shows that the number of readings for the winter in total does not significantly differ from the spring or summer amounts. Fall has fewer measurements due to the small number of readings available for October 1997. Given the sheer number of observations in all seasons, their ranges, and the consistency of their distribution, the results shown in the table and graphs appears reliable even without many October readings. While these results were obtained using the seasons as defined by the calendar rather than extending the winter season from November to April and shifting summer to include June through September, these results are consistent with those found by Makshtas et al. (1998).

	Cloud Coverage (any height clouds) by season and coverage in tenths						
	Count	<0.3	0.3-0.499	0.5-0.699	0.7-0.899	0.9-1.0	No Data
Winter							
Count	1817	826	31	61	78	762	59
Percent		45.5	1.7	3.4	4.3	41.9	3.2
Spring							
Count	2139	247	39	72	91	1662	28
Percent		11.6	1.8	3.4	4.3	77.7	1.3
Summer							
Count	2139	169	43	48	94	1785	0
Percent		7.9	2.0	2.2	434.0	86.5	0.0
Fall							
Count	1357	338	29	35	54	867	34
Percent		24.9	2.1	2.6	4.0	63.9	2.5

Table 1. Cloud coverage for the four season during the entire SHEBA measurement period.

Monthly results show that the winter trend of nearly equal distributions of clear and overcast sky readings is present in December, January and February (Figure 6). Clear skies begin to decrease in frequency after February until a minimum is reached in August, continuing in September (Figure 7). Unfortunately, the lack of data during October doesn't permit any conclusion about the cloudiness during that month, but of the 22 readings, it is notable that there are no readings below 8 tenths (Figure 8). Clear sky occurrences begin to increase again in November (Figure 8). A histogram of cloud coverage for the entire year, broken down by month, illustrates this distribution well (Figure 9).

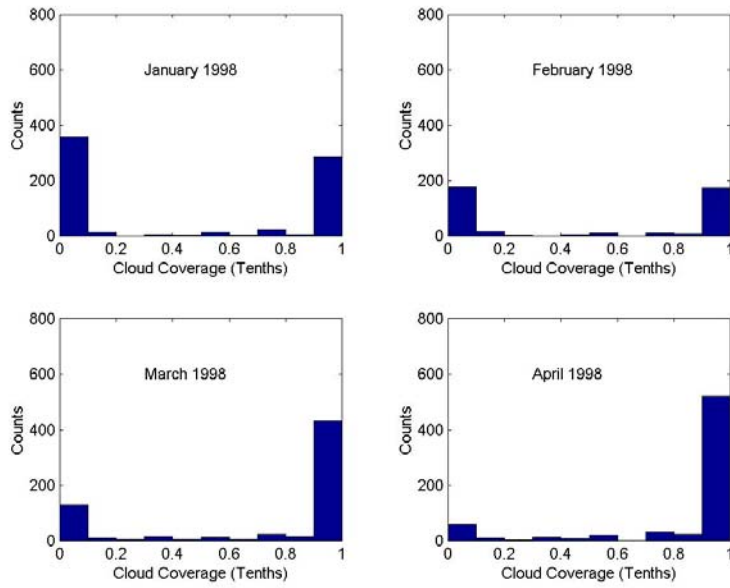


Figure 6. Cloud coverage by month depicting number of occurrences for each cloud coverage level in tenths.

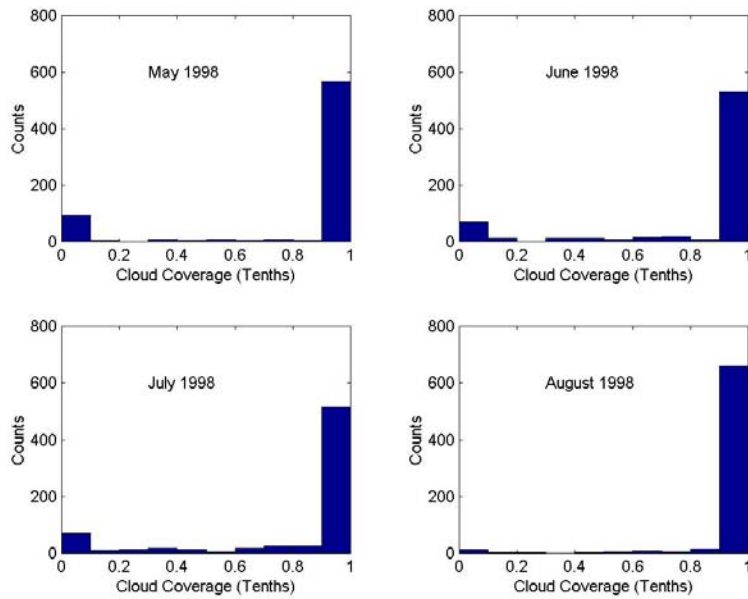


Figure 7. Cloud coverage by month depicting number of occurrences for each cloud coverage level in tenths.

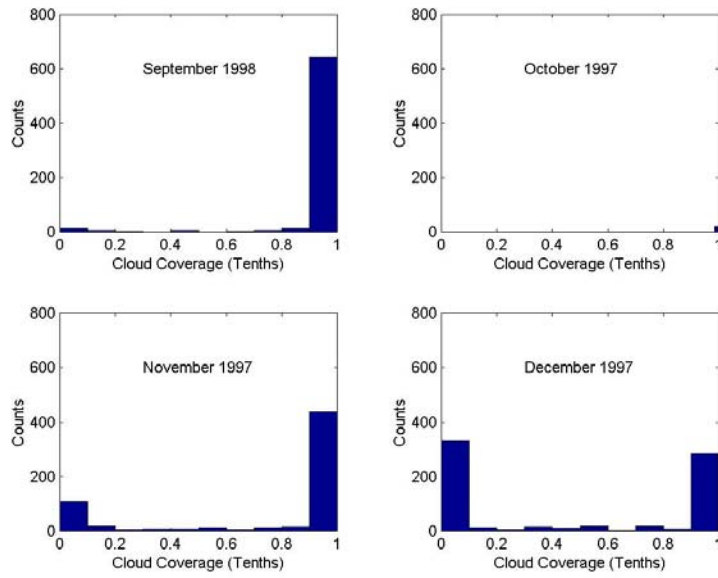


Figure 8. Cloud coverage by month depicting number of occurrences for each cloud coverage level in tenths.

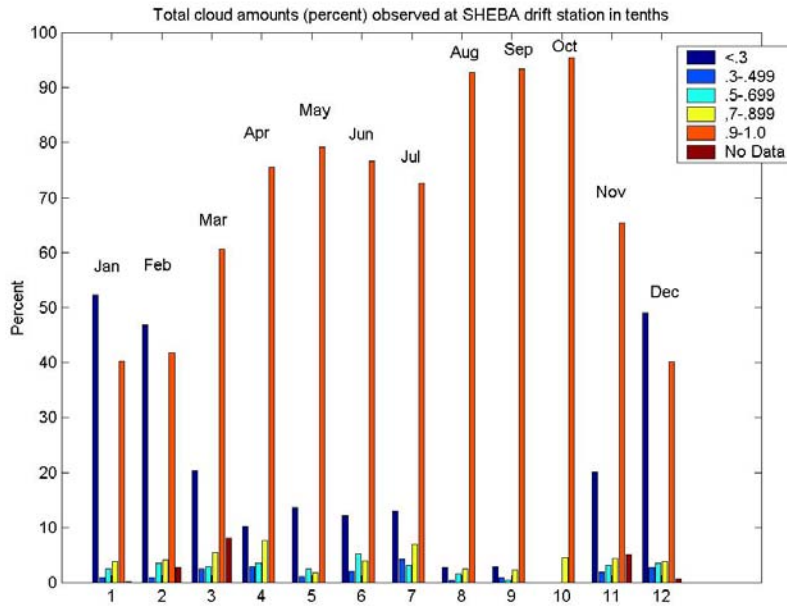


Figure 9. Histogram of cloud coverage for all cloud heights by month and tenths for entire SHEBA measurement period.

The occurrences of low clouds, considered to be those at less than 5000 ft (1524 m) as measured to the cloud base-height, have a slightly different distribution (Figure 10). In the winter months there are fewer instances of low clouds than in spring and summer months. These values are close, though lower in winter and higher in summer compared to Makshtas et al. (1998).

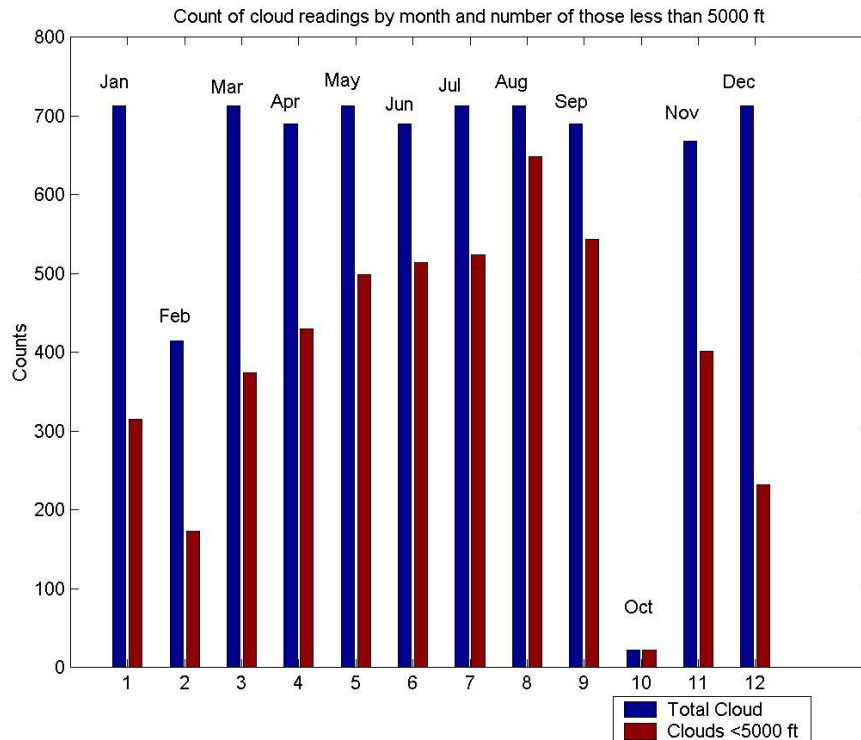


Figure 10. Cloud coverage by month for entire SHEBA measurement cycle, depicting number of cloud measurements taken and those that were low clouds (cloud base height less than 5000 feet or 1524 meters).

The above results can be misleading however, as there are far fewer instances of clouds, regardless of height, in the winter months as demonstrated above. When the percentage of readings where clouds are present is compared with the percentage of low clouds, there is a different distribution (Figure 11). Figure 11 illustrates only those readings in which there was some cloud coverage registered. Completely clear days are not included in this graph.

Figure 11 shows that when low clouds were present, at least 78% of the readings showed overcast skies of at least 9 tenths coverage (Figure 11). In other

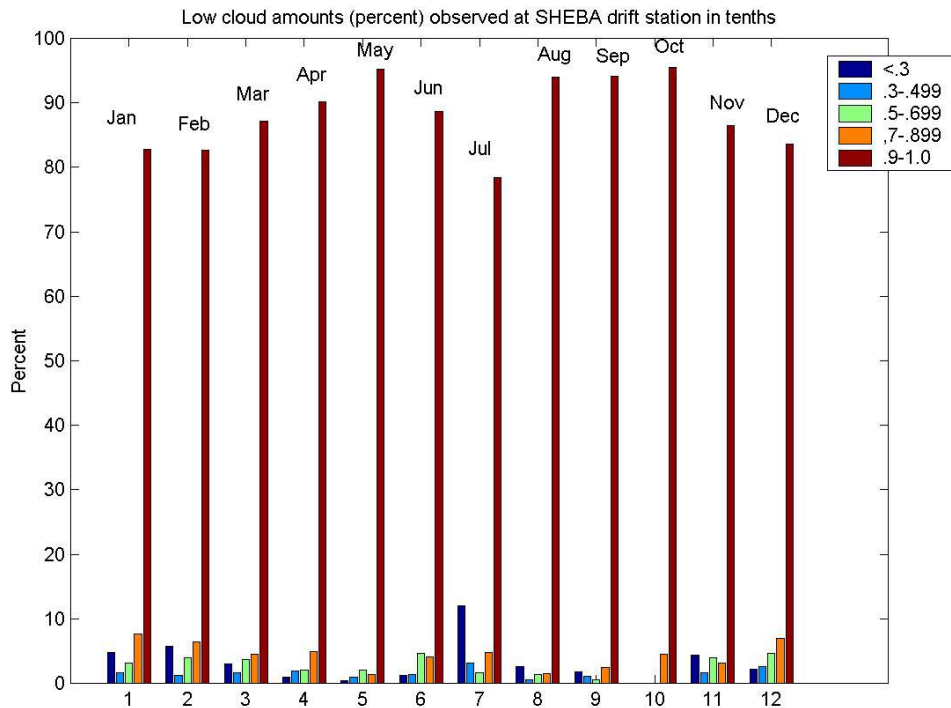


Figure 11. Percent of low cloud coverage in non-clear conditions (defined as cloud coverage greater than 0).

words, when low clouds were present at all, the skies were predominantly overcast, regardless of how many days during a month were clear of clouds, or the month of the year. This matches the visual observations of those present during the collection of the SHEBA data and personal experience from those who have been in the Arctic region in this area. Table 2 gives the number and percentage of observations for low-level cloud in several categories of cloud fraction.

Division of the cloud heights into four groups, depicting the distribution of cloud bottom height, shows the relative occurrences for low, mid-level, high and very high clouds against the frequency of clear skies for the entire measurement period (Figure 12). This graph also shows that low clouds occur more than

twice as often as clear skies with mid and upper level clouds being the least observed base cloud height.

Cloud Coverage (low clouds <5000 ft) by month and coverage in tenths							
	Total Counts	<0.3	0.3-0.499	0.5-0.699	0.7-0.899	0.9-1.0	No Data
January							
Count	713	413	5	10	24	261	0
Percent(low)	44.2	57.9	0.7	1.4	3.4	36.6	0.0
February							
Count	414	251	2	7	11	143	0
Percent(low)	41.8	60.6	0.5	1.7	2.7	34.5	0.0
March							
Count	713	350	6	14	17	326	0
Percent(low)	52.5	49.1	0.8	2.0	2.4	45.7	0.0
April							
Count	690	264	8	9	21	388	0
Percent(low)	62.3	38.3	1.2	1.3	3.0	56.2	0.0
May							
Count	713	217	5	10	7	474	0
Percent(low)	69.8	30.4	0.7	1.4	1.0	66.5	0.0
June							
Count	690	182	7	24	21	456	0
Percent(low)	74.5	26.4	1.0	3.5	3.0	66.1	0.0
July							
Count	713	252	16	9	25	411	0
Percent(low)	73.5	35.4	2.2	1.3	3.5	57.6	0.0
August							
Count	713	82	3	9	10	609	0
Percent(low)	90.9	11.5	0.4	1.3	1.4	85.4	0.0
September							
Count	690	157	6	3	13	511	0
Percent(low)	78.7	22.8	0.8	0.4	1.9	74.1	0.0
October							
Count	22	0	0	0	1	21	0
Percent(low)	100.0	0.0	0.0	0.0	4.5	95.5	0.0
November							
Count	668	285	7	16	13	347	0
Percent(low)	60.0	42.7	1.0	2.4	1.9	51.9	0.0
December							
Count	713	486	6	11	16	194	0
Percent(low)	32.5	68.2	0.8	1.5	2.2	27.2	0.0

Table 2. Cloud coverage in count and percent for low clouds. Each count is one reading of cloud base height by ceilometer or LIDAR for that month. Total count is the number of total readings, regardless of amount of coverage.

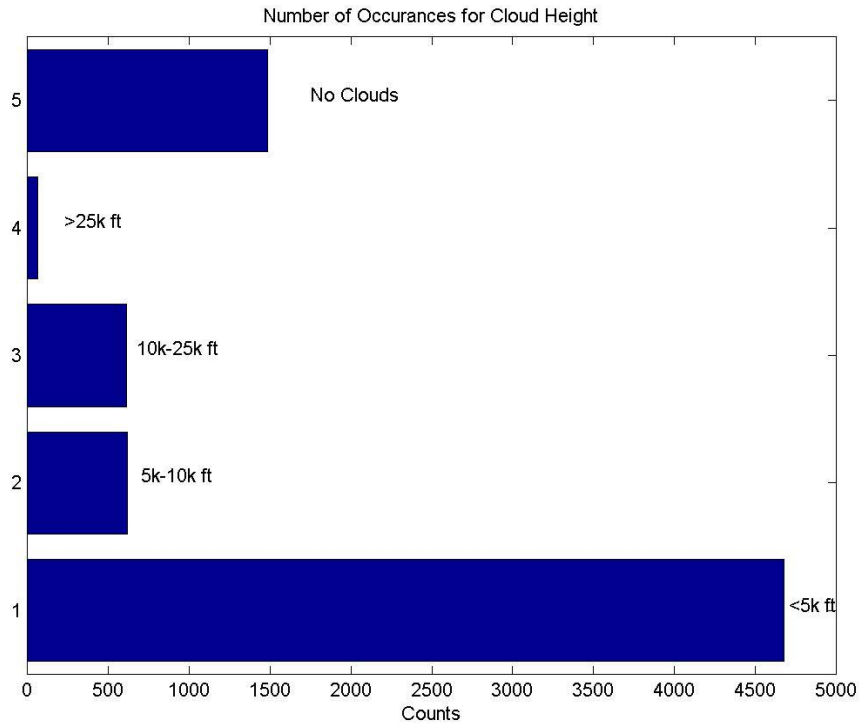


Figure 12. Histogram of the number of occurrences of clouds by cloud height.

Again, the limitations of the SHEBA data are that the cloud measurements are restricted to coverage and cloud base height. There are no data available giving cloud thicknesses; therefore multiple levels of clouds are not accounted for in these graphs and tables. It is quite likely that mid and upper level clouds were present in many instances but were not registered due to the overcast nature of the skies at the low cloud level.

Of concern is that the SHEBA drift camp was drifting over a large area during the measurement period, and that the results may not reflect any specific area accurately. In Makshtas et al. (1998), the area of coverage includes much of the SHEBA area, and some of the surrounding areas (Figures 1 & 13).

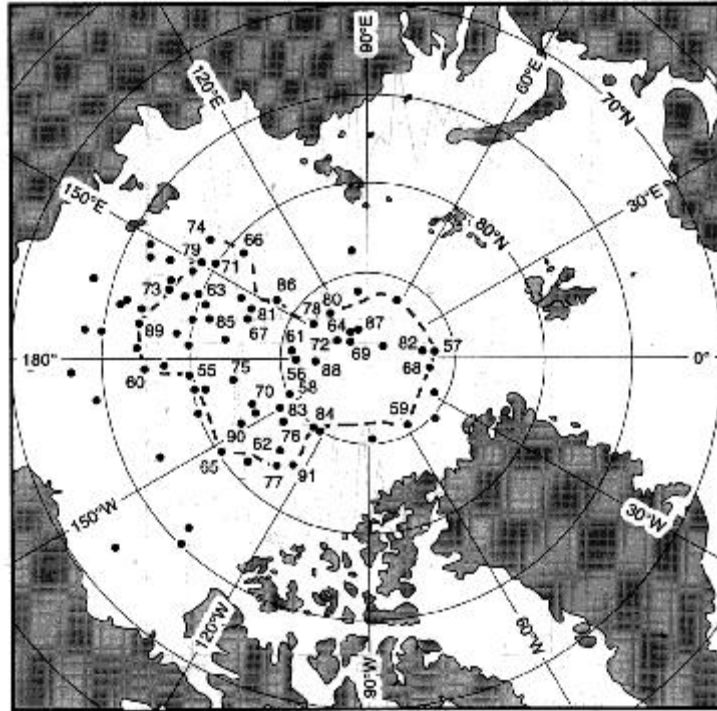


Figure 13. From Makshtas et al., (1998), depicting area of study. Limits of study are bounded by dashed line. SHEBA study area, shown in Figure 1., was in much the same area.

Because the results presented here are consistent with their results, the SHEBA data appears to be representative of a large area of the western Arctic that is away from continental and open-ocean influences. Since the nature of the surface tends toward homogeneity on large scales, with snow and ice in winter and melt ponds, leads and fractures appearing in summer throughout much of the central basin, it is reasonable to expect that measurements will be applicable to a larger area than that immediately surrounding the instruments performing the measurements.

B. LONGWAVE RADIATION

A time series of the net longwave radiation for the 11-month SHEBA measurement period shows many rapid jumps associated with variations in sky conditions (Figure 14). Sky conditions often changed from cloudless to completely overcast or vice versa from one hour to the next.

The convention of signs in this study is such that a positive net radiation indicates a surface heat loss (i.e. positive upwards). Mean net longwave radiation, LW↓ for the entire period was 18.91 W/m², which included all sky conditions. Completely overcast skies occurred 67.9% (4,026 hours) of the time with a mean LW↓ of 10.06 W/m². Completely clear skies occurred 19.6% (1,159 hours) of the time with a mean LW↓ of 44.71 W/m². Partially cloudy skies occurred 12.5% (742 hours) of the time with a mean LW↓ 25.13 W/m².

These net longwave radiation values are significantly lower than those reported during the Antarctic ANZFLUX experiment, which took place in the austral winter (Guest, 1998). For each sky condition, ANZFLUX measurements reported nearly twice the amount recorded here even though the relative frequency of the sky conditions was very similar (Guest, 1998).

An examination of the net longwave radiation flux by sky condition shows the distribution of the net flux (Figure 15). Of all clear sky readings, 84.5% occurred during the cool half of the year, (October-April), with an average LW↓ of 40.60 W/m². The remaining 15.5% of clear sky readings occurred in the warm half of the year, (May-September), and had an average LW↓ of 67.04 W/m². For completely overcast readings, 47.7% occurred in the cool half of the year with an average LW↓ of 12.81 W/m² and 52.3% occurred in the warm half with an average LW↓ of 7.56 W/m². Of those readings in which the sky was between clear and completely overcast, 55.9% occurred in the cool half an averaged LW↓ of 28.58 W/m² and 44.1% occurred in the warm half with an average LW↓ of 20.75 W/m².

Even comparing only the flux averages for the cool half of the year with those reported for ANZFLUX during the austral winter, the net flux is still only approximately half of those southern hemisphere averages (Guest, 1998).

Differences between the net values reported here and those reported during ANZFLUX are not an unexpected result. For comparison, ANZFLUX gathered their measurements over the Weddell Sea in the Antarctic (Guest, 1998). The Weddell Sea has a very different character, despite them both being

in polar regions, than the SHEBA area in the Beaufort Sea. The Weddell Sea is characterized by warmer waters just below the surface, contributing thermal energy to the surface of the water and inhibiting the formation and thickening of sea ice there. The Beaufort Sea, in the SHEBA measurement area, is an area of thick ice development and year round ice coverage in many areas (Guest, 1998 & Persson, 2001).

In the height of cloud bases, there is a difference in these areas as well. As was discussed in the cloud chapter, the cloud bases in the Beaufort Sea tend to be low (Makshtas et. al., 1998). In the Weddell Sea, especially in winter, the cloud bases tend to be higher than those recorded in the Arctic (Guest, 1998). Since the downward component of the longwave radiation depends on temperature, a higher cloud base results in lower temperatures, decreasing the downward longwave radiation. Given this relationship, it is natural to expect a greater positive net longwave radiation, indicating a greater surface heat loss in the Antarctic than in the Arctic.

While an in depth explanation of the differences between these two areas is not feasible here, the above differences do lead to the expectation that measurements of many meteorological variables as well as net longwave and shortwave radiation totals would be significantly different. Other possible explanations, proof of which is beyond the scope of this paper, include the potential for greater aerosols in the Arctic. Whether in the form of diamond dust or pollution from North America and the Russian states, this may account for an artificial increase in downward longwave radiation values resulting in a net lower longwave radiation flux (Overland and Guest, 1991).

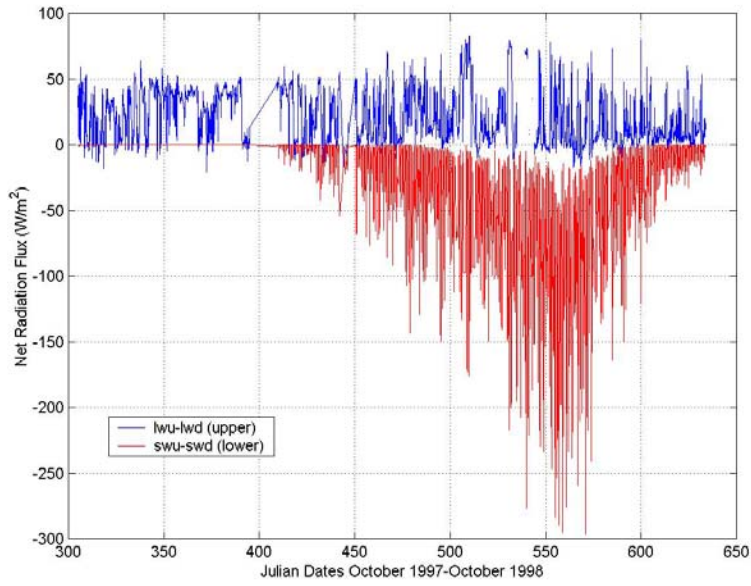


Figure 14. Time series of the net measured radiation flux (W/m^2). January 1, 1998 is given the Julian date of 366.

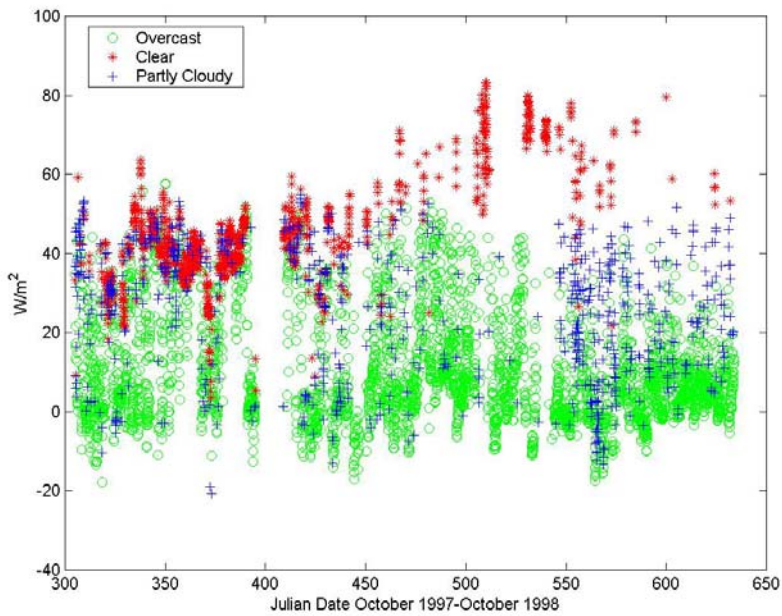


Figure 15. Net longwave radiation flux by cloudiness level. Net flux is calculated by longwave upward-downward. Partly cloudy skies have cloudiness percentages $>0\%$ and $<100\%$.

The correlations between cloud cover, air temperature and downward longwave radiation, $LW\downarrow$, lend themselves to inclusion in parametric equations (Guest, 1998). This correlation is well depicted through a scatter plot of surface temperature expressed as blackbody radiation and $LW\downarrow$ (Figure 16). All measurements were divided into cases in which the sky was completely free of clouds, completely overcast and skies with cloudiness fractions between the two extremes for comparison with the results of the parametric equations tested in this study.

At the lower temperature and longwave downward radiation values, there is a great deal of overlap (Figure 16). This indicates that the impact of cloud coverage means less at the lowest temperatures.

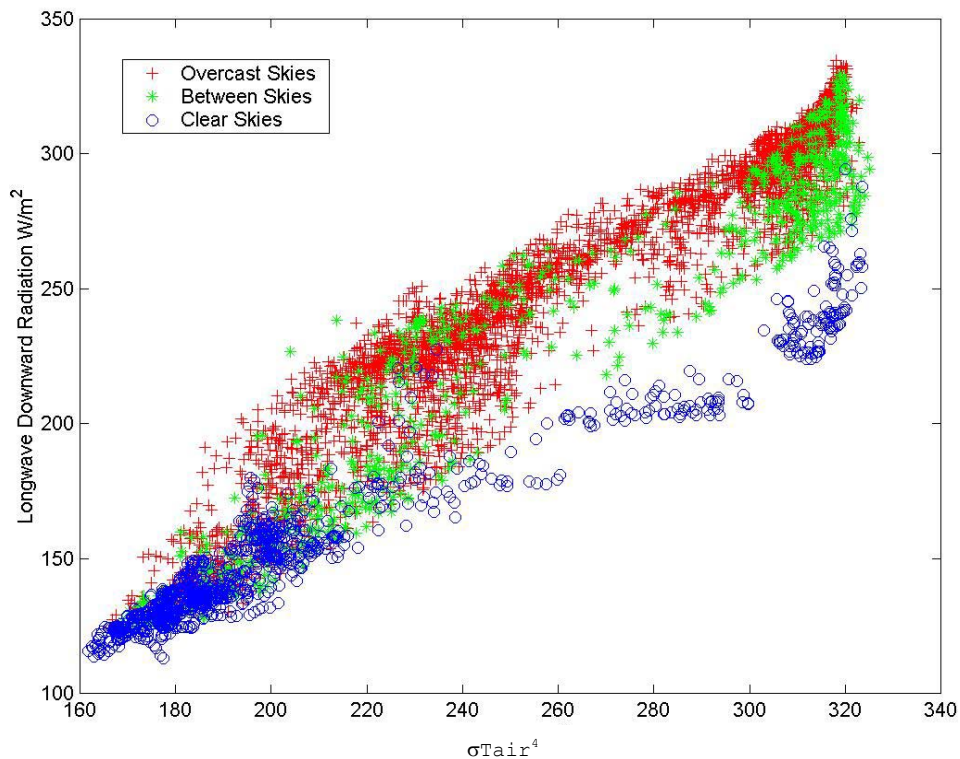


Figure 16. Surface temperature expressed as blackbody radiation (σT_{air}^4) vs. measured longwave radiation for completely clear skies, completely overcast skies and partly cloudy skies.

1. Clear Sky Downwelling Longwave Radiation

Fifteen published parametric formulas for longwave downwelling radiation under clear sky conditions were tested with the SHEBA dataset (Table 3). In the tables, statistical entries for the “Mean Error” refer to the mean of all 1,159 differences between the predicted and measured values for longwave downward radiation, $LW\downarrow$, and represents bias errors. “Standard Deviation” refers to the standard deviation of the difference between observed and predicted values and represents scatter or random-like errors. “Total Error” is the root-mean squared (rms) value of the differences and includes both bias-type and random-type errors (Table 4).

Efimova(1961)	$LW\downarrow (clear) = \sigma T_{air}^4 (0.746 + 0.0066e)$
Maykut & Church(1973)	$LW\downarrow (clear) = \sigma T_{air}^4 (0.7855)$
Marshunova(1966)	$LW\downarrow (clear) = \sigma T_{air}^4 (0.67 + 0.05e^{0.5})$
Idso(1981)	$LW\downarrow (clear) = \sigma T_{air}^4 (0.70 + 5.95 \times 10^{-5} e^{1500/T_{air}})$
Ohmura(1981)	$LW\downarrow (clear) = \sigma T_{air}^4 (8.733 \times 10^{-3} T_{air}^{0.788})$
Idso & Jackson(1969)	$LW\downarrow (clear) = \sigma T_{air}^4 [1 - 0.261 \exp\{-7.77 \times 10^{-4} (273 - T_{air})^2\}]$
Guest(1998)(*const)	$LW\downarrow (clear) = \sigma T_{air}^4 (0.6309)$
Andreas & Ackley(1982)	$LW\downarrow (clear) = \sigma T_{air}^4 (0.601 + 5.95 \times 10^{-5} e^{1500/T_{air}})$
Guest(1998)(e)	$LW\downarrow (clear) = \sigma T_{air}^4 (0.3353 + 0.1952e^{0.5}) + 25.5$
Guest(1998)) – const)	$LW\downarrow (clear) = \sigma T_{air}^4 - 85.6$
Guest(1998)(RHi)	$LW\downarrow (clear) = \sigma T_{air}^4 1.1024 + 0.2484RH_i - 131.1$
Guest(1998)(RH)	$LW\downarrow (clear) = \sigma T_{air}^4 1.0438 + 0.2486RH - 113.6$
Swinbank(2nd)(1963)	$LW\downarrow (clear) = \sigma T_{air}^4 (9.365 \times 10^{-6} T_{air}^2)$
Zillman(1972)	$LW\downarrow (clear) = \sigma T_{air}^4 (9.2 \times 10^{-6} T_{air}^2)$
Swinbank(1st)(1963)	$LW\downarrow (clear) = \sigma T_{air}^4 1.195 - 170.9$

Table 3. Various parameterizations for clear sky downwelling longwave radiation.

Clear Sky LWd - All Seasons	Mean Error	Standard Deviation	Total Error
1159 points			
Efimova 1961	0.949	8.928	8.978
Maykut and Church 1973	7.325	8.708	11.379
Marshunova 1966	-7.108	10.287	12.504
Idso 1981	-10.019	9.231	13.623
Ohmura 1981	-16.277	8.964	18.581
Idso and Jackson 1969	21.140	14.662	25.727
Guest 1998 (*constant)	-24.536	11.017	26.896
Andreas and Ackley 1982	-25.951	9.033	27.478
Guest 1998 (e)	-23.373	22.679	32.567
Guest 1998 (-constant)	-34.070	12.819	36.402
Guest 1998 (RH _i)	-33.485	15.444	36.875
Guest 1998 (RH)	-33.887	15.331	37.194
Swinbanks second 1963	-36.326	10.664	37.859
Zillman 1972	-38.409	10.303	39.767
Swinbanks first 1963	-79.183	19.943	81.656

Table 4. Mean Error, Standard Deviation and Total Error between measured longwave radiation and parametric equations for completely clear skies. Bold indicates the best three formulas. Negative values indicate predicted values were less than measured values.

Of the fifteen formulas, there was a great deal of variation in the total error, with Maykut & Church (1973), Efimova (1961) and Marshunova (1966) having the least total error. Some of the formulas used in this paper were not formulated with data from the Arctic, specifically those from the recent ANZFLUX experiment in the Antarctic (Guest, 1998) and those taken from Zillman (Zillman, 1972). The relative performance of these equations with data from the Arctic was of interest for this study and, as shown in Table 4, their performance was of similar, or better, accuracy than some Arctic derived formulas.

The three best performing parametric formulas were all formulated for the Arctic. Scatter error patterns for each of the three best formulas resemble each other closely, as do their error statistics (Figure 17 & Table 4). Efimova's (1961) and Marshunova's (1966) formulas, which were the first and third best of all clear sky parametric formulas, used vapor pressure (e) along with blackbody

temperature in the formula. Maykut & Church's (1973) used only a simple numerical modifier of temperature and was almost equally accurate in predicting $LW\downarrow$. All equations assumed knowledge that skies were completely clear of clouds.

A time series of those three formulas shows how close these formulas predicted the actual measured $LW\downarrow$ on a daily basis throughout the measurement cycle (Figure 18). Graphs of the scatter plots for error and the time series graphs for all fifteen clear sky parametric formulas are found in Appendix A (Figures A1-A8).

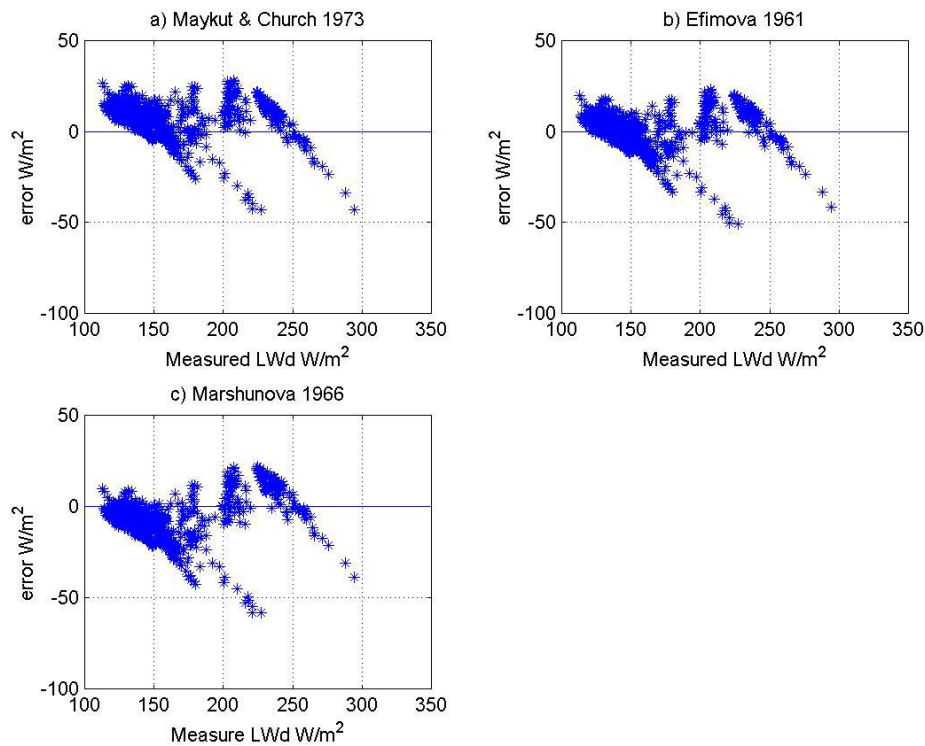


Figure 17. Measured and parameterized $LW\downarrow$ (LWd) from the three most accurate parametric equations during completely clear skies with 1159 hourly points.

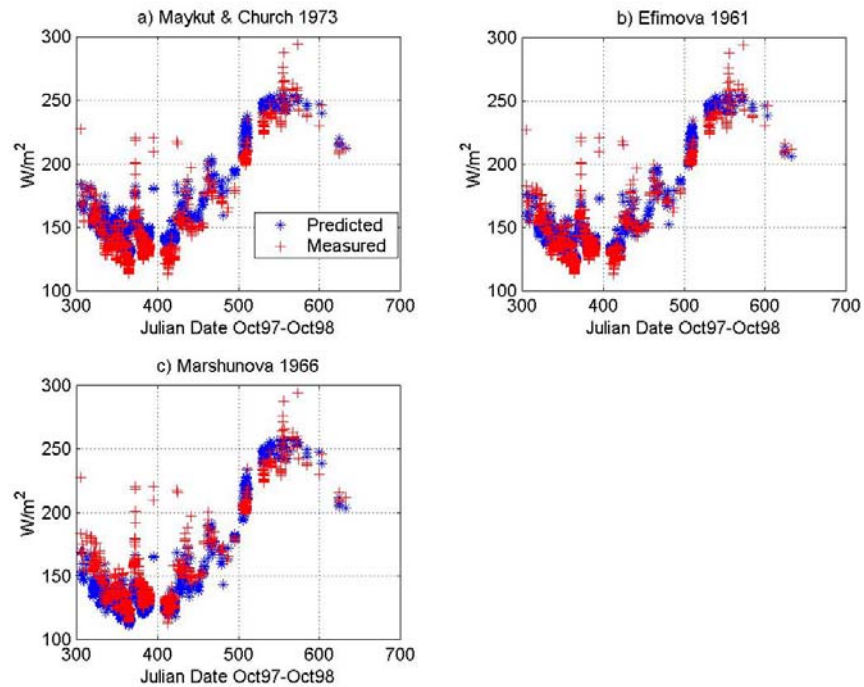


Figure 18. Time series showing the predicted LW↓ and the measured LW↓ for the three best performing parametric equations.

2. Overcast Sky Longwave Downwelling Radiation

During periods in which the cloud coverage was 100%, (completely overcast), measured longwave downwelling radiation was compared with ten previously published parametric formulas (Table 5). A total of 4,026 points out of 5,927 total points represented overcast periods, and were included in this portion of the study.

Of the ten formulas tested, the four most accurate were Maykut & Church (1973), Key et al. (1996), Guest (using RH) and Guest (using RHi) (1998) (Figure 19). Unlike the clear sky parametric equations, there wasn't a great deal of variation in the accuracy of the formulas (Tables 4 & 6). Comparison of the "Total Error" for both cases describes these differences.

Key et al(1996)	$LW \downarrow (\text{overcast}) = \sigma T_{\text{air}}^4 1.26(0.746 + 0.0066e)$
Guest(1998)(RH _i)	$LW \downarrow (\text{overcast}) = \sigma T_{\text{air}}^4 1.0426 + 0.5320RH_i - 78.4$
Guest(1998)(RH)	$LW \downarrow (\text{overcast}) = \sigma T_{\text{air}}^4 0.9327 + 0.5731RH - 47.3$
Maykut & Church(1973)	$LW \downarrow (\text{overcast}) = \sigma T_{\text{air}}^4 (0.96)$
Guest(1998)(e)	$LW \downarrow (\text{overcast}) = \sigma T_{\text{air}}^4 (1.1103 - 0.01181e^{0.5}) - 43.4$
Zillman(1972)	$LW \downarrow (\text{overcast}) = \sigma T_{\text{air}}^4 \{9.2 \times 10^{-6} T_{\text{air}}^2 + .96(1 - 9.2 \times 10^{-6} T_{\text{air}}^2)\}$
Guest(1998)) – const)	$LW \downarrow (\text{overcast}) = \sigma T_{\text{air}}^4 - 18.7$
Guest(1998)(*const)	$LW \downarrow (\text{overcast}) = \sigma T_{\text{air}}^4 (0.9304)$
Marshunova(1966)	$LW \downarrow (\text{overcast}) = \sigma T_{\text{air}}^4 1.31(0.67 + 0.05e^{0.5})$
Parkinson & Washington(1979)	$LW \downarrow (\text{overcast}) = \sigma T_{\text{air}}^4 1.3[1 - 0.261 \exp\{-7.77 \times 10^{-4} (273 - T_{\text{air}})^2\}]$

Table 5. Parametric equations tested for overcast skies.

Overcast Sky LWd 4026 Points	Mean Error	Standard Deviation	Total Error
Key et al. 1996	2.660	14.399	14.643
Guest 1998 (RH _i)	-3.580	14.203	14.647
Guest 1998 (RH)	-3.463	14.490	14.898
Maykut & Church 1973	0.308	15.717	15.720
Guest 1998 (e)	-8.417	14.203	16.510
Zillman 1972	7.089	15.049	16.635
Guest 1998 (- constant)	-7.710	14.939	16.811
Guest 1998 (* constant)	-7.598	16.390	18.065
Marshunova 1966	-10.278	17.403	20.212
Parkinson & Washington 1979	13.244	23.784	27.223

Table 6. Mean Error, Standard Deviation and Total Error between measured longwave radiation and parametric equations for occurrences of completely overcast skies. Bold indicates the best four parametric formulas.

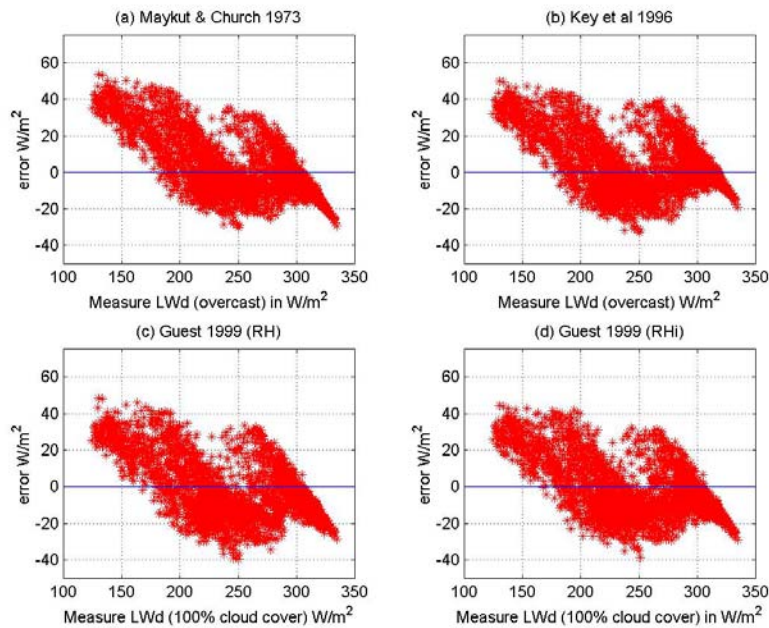


Figure 19. Most accurate parametric equations for LW↓ during completely overcast skies with 4026 hourly points.

Of note is that the Guest (1998) equations were formulated with data from the Antarctic while the other two were created from Arctic data sets. Guest's formulas use the relative humidity with respect to ice or the relative humidity along with a modifier to the air temperature (Guest, 1998). Key et al. (1996) uses e with air temperature. Of the four best, only Maykut & Church's uses only a modifier of air temperature near the surface. All formulas assumed knowledge that the cloud coverage was completely overcast.

With all the formulas tested one might expect that the more variables that are included, the more accurate the equation will be. However, this wasn't the case under overcast skies. The improvement in skill of the equations using variables other than surface temperature and cloud cover did not result in a significant improvement in accuracy. The difficulties associated with measuring, on a consistent basis, any variable near the surface in the Arctic using remote means makes many of the parametric formulas unwieldy for use with a model. For this reason, Maykut & Church's (1973) equation, which uses only a linear

modifier of surface temperature, remains the best in terms of accuracy and ease of use with models.

This is especially true in view of the very small differences between the accuracies of the best four formulas regardless of the number of measured variables included in the formula. A time series showing the predicted and measured $LW\downarrow$ throughout the measurement cycle for these formulas depicts the successful daily predictions they were capable of (Figure 20). A full set of graphs depicting the error scatter plots and the time series graphs of the overcast measurements for all eleven parametric equations is included in Appendix A (Figures A9-A14).

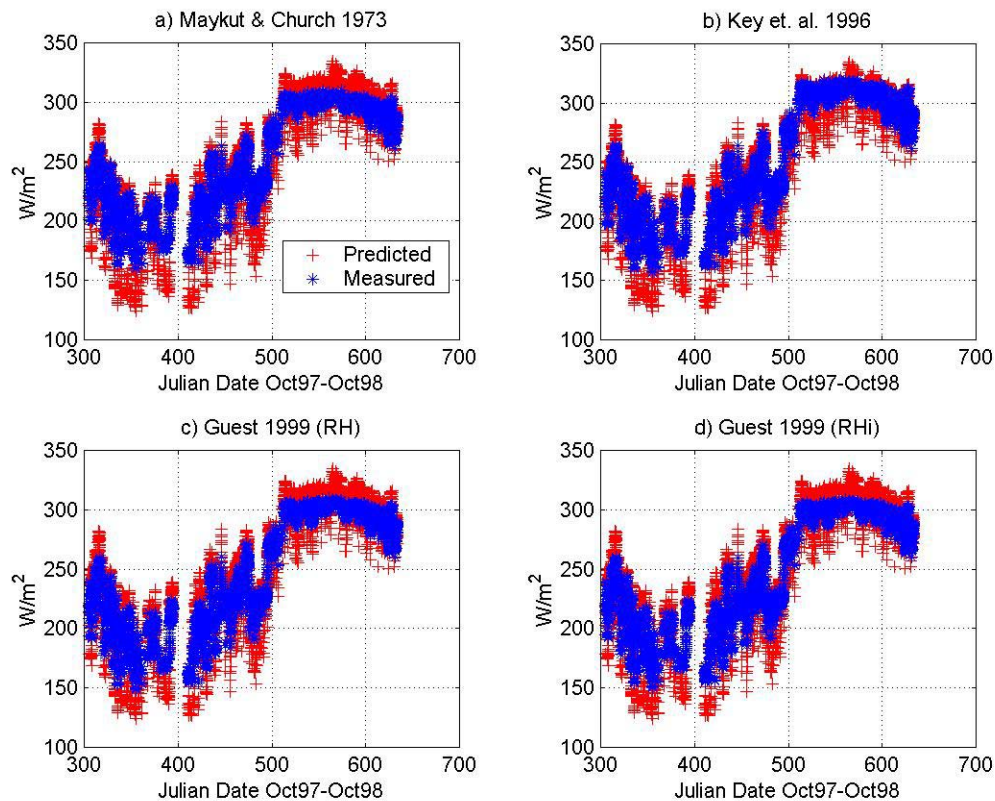


Figure 20. Time series of the four best parametric formulas under overcast conditions. Each graph has the predicted $LW\downarrow$ (red +) and the measured $LW\downarrow$ (blue *) for each hourly measurement.

3. Partly Cloudy Sky Longwave Downwelling Radiation

Five formulas were evaluated testing with partly cloudy skies (Table 7). For purposes of this study, any cloud coverage percentage greater than zero, but less than 100% is termed as partly cloudy. In total, 742 out of 5,927 hourly measurements were classified in this category. Percentages of cloud cover ranged from 0.4% to 99.5%.

The variation in the prediction accuracy of the tested equations was not great (Table 8). The range of accuracies was more like that of overcast rather than clear skies.

The best three performing of the formulas were Maykut & Church (1973), Efimova (with the Jacobs cloud correction as recommended by Key et. al. 1996) (1961) and Marshunova (1966) (Table 5). All three were formulated for the Arctic. Scatter of the error for the three best give an indication of how well the formulas predict the measured $LW\downarrow$ overall, but that individual readings may be more than 50 W/m^2 in error (Figure 21). Examination of the scatter plots and time series shows that, like the overcast data, the spread of error is relatively evenly distributed on both sides of zero (Figures 21 & 22). The size of the error, as shown in the standard deviations, is greater than that recorded for overcast skies (Table 5). This is likely due to the wide range of values that fall into the partly cloudy range and the fact that an entire yearly cycle passed during the measurements.

For the three best formulas, only Maykut & Church's (1973) equation uses only air temperature, (expressed as a blackbody radiation), and a percentage of cloud cover. This is precisely the same result arrived at for overcast and clear skies. Full sets of graphs showing the scatter error plots and time series graphs for all five parametric is included in Appendix A (Figures A15-A18).

Maykut & Church(1973)	$LW \downarrow (\text{overcast}) = \sigma T_{\text{air}}^4 (0.7855(1 + 0.22232(c^{2.75})))$
Zillman(1972)	$LW \downarrow (\text{overcast}) = \sigma T_{\text{air}}^4 \{9.2 \times 10^{-6} T_{\text{air}}^2 + .96(1 - 9.2 \times 10^{-6} T_{\text{air}}^2)\}c$
Marshunova(1966)	$LW \downarrow (\text{overcast}) = \sigma T_{\text{air}}^4 1.31(0.67 + 0.05e^{0.5})(1 + c1 * c)$
Efimova 1961 (with Jacobs cloud correction from Key et al 1996)	$LW \downarrow (\text{partly}) = \sigma T_{\text{air}}^4 (0.746 + 0.0066e)(1 + 0.26c)$
Parkinson & Washington(1979)	$LW \downarrow (\text{overcast}) = \sigma T_{\text{air}}^4 [1 - 0.261 \exp\{-7.77 \times 10^{-4} (273 - T_{\text{air}})^2\}](1 + 0.3c)$
$c = \text{cloud fraction}$	

Table 7. Parametric equations for partly cloudy skies.

Party Cloudy Sky Longwave 742 points	Mean Error	Standard Deviation	Total Error
Marshunova 1966	-6.029	19.474	20.386
Efimova 1961 (with Jacobs cloud correction from Key et. al. 1996)	5.579	20.213	20.969
Maykut & Church 1973	-3.702	21.644	21.958
Zillman 1972	-4.006	26.118	26.423
Parkinson & Washington 1979	15.549	29.877	33.681

Table 8. Mean Error, Standard Deviation and Total Error between measured longwave radiation and parametric equations for occurrences of partly cloudy skies. The three best of the formulas are in bold.

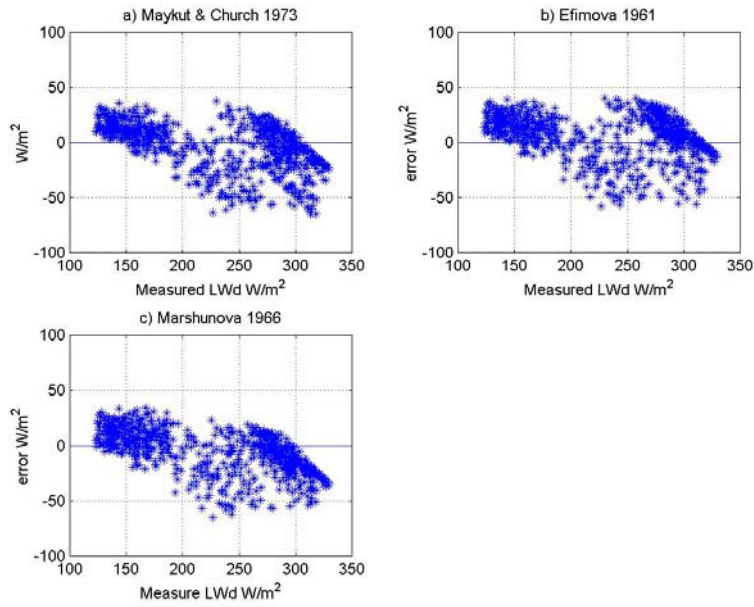


Figure 21. Scatter plot of error for three best prediction equations for $LW\downarrow$ under partly cloudy sky conditions.

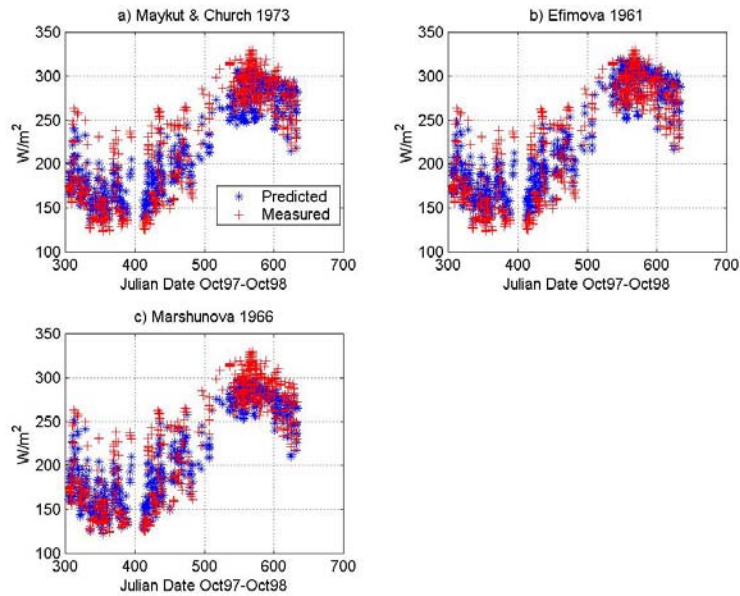


Figure 22. Time series of predicted and measured $LW\downarrow$ for the three best prediction equations under partly cloudy skies.

C. SHORTWAVE RADIATION

A time series of net shortwave radiation, $SW\uparrow$, throughout the measurement period shows the annual cycle of solar radiation for this Arctic region (Figure 14). Mean $SW\uparrow$ for the period for clear sky conditions was -17.76 W/m^2 . Completely overcast skies had a mean $SW\uparrow$ of -23.33 W/m^2 . Under partly cloudy conditions, in which the cloud percentage ranged from 0.4% to 99.5%, the mean $SW\uparrow$ was -46.49 W/m^2 . These net shortwave radiation means included the polar night period when no shortwave radiation was included in the mean.

Under partly cloudy conditions, the cool half of the year (October-April) mean $SW\uparrow$ was -8.03 W/m^2 and the warm half (May-September) was -75.80 W/m^2 . For clear skies the cool half mean $SW\uparrow$ was -2.86 W/m^2 and the warm half was -83.40 W/m^2 . During completely overcast conditions, the mean $SW\uparrow$ was -5.85 W/m^2 during the cool half and -41.52 W/m^2 for the warm half.

Because the amount of radiation reaching the surface depends on the angle of the rays, it is natural that there be a strong correlation between the solar zenith angle and $SW\downarrow$ (Figure 23). It is clearly seen that there is a strong line of best fit for $SW\downarrow$ under clear skies, which lies along a line at the top of all values (Figure 23). Under overcast skies there is a great deal of scatter that increases as the angle of the sun above the horizon decreases, meaning the sun shining more overhead (Figure 23). As the sun rises higher in the sky, the more direct the path the light takes through the layers of clouds, thereby being less affected by the scattering effects of the clouds.

Figure 24 depicts the relationship between the $SW\downarrow$ and the cloud amount. It illustrates the rapidly changing nature of the sky conditions throughout the measurement cycle. Though there is light visible after the sun has passed the 90° angle, (i.e. sunset), any solar zenith angle greater than 90° was omitted from use in the parametric equations which follow. The solar constant, s_0 , used in the parametric equations was 1367 W/m^2 (Garratt, 1992).

In a world without an atmosphere or any matter between the sun and the surface, calculation of the downward shortwave radiation could be accurately calculated for any time and location. In the presence of our atmosphere and its clouds, aerosols and wind blown debris, the problem is much more complicated. Each of the parametric equations tested required knowledge of the latitude and longitude as well as a time in order to calculate the solar zenith angle. Some of the equations required other variables such as e (vapor pressure) while others make only a numerical modification of the solar constant using the solar zenith angle.

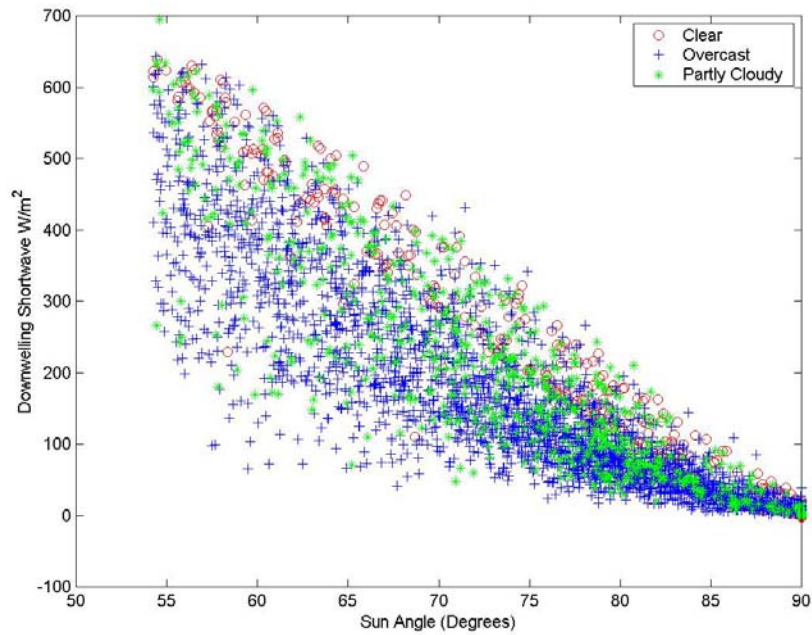


Figure 23. Scatter plot of the angle of the sun above the horizon and measured downward shortwave radiation.

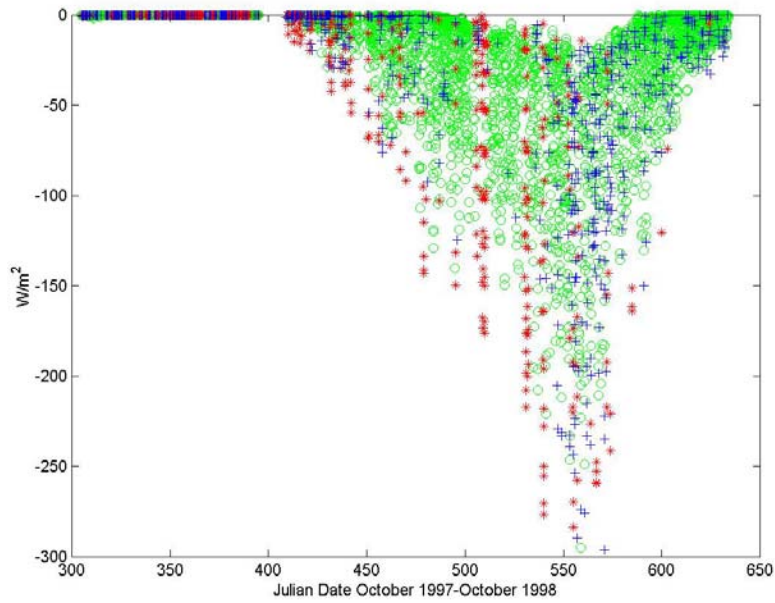


Figure 24. Time series of the measured SW↓ (W/m2) by sky condition.

1. Clear Sky Downwelling Shortwave Radiation

Nine previously published parametric equations were tested using the SHEBA data set (Table 9). Error parameters are the same as those described for longwave radiation tables. Like the results for clear sky LW↓, SW↓ error statistics showed a great deal of variation (Table 10).

Zillman (1972)	$SW \downarrow = S_0 \cos(Z)^2 / (1.085 \cos(Z) + (2.7 + \cos(Z))10^{-3} e + 0.10)$
Shine (1984)	$SW \downarrow = S_0 \cos(Z)^2 / (1.2 \cos(Z) + (1.0 + \cos(Z))10^{-3} e + 0.0455)$
Bennett (1982)	$SW \downarrow = S_0 0.72 \cos(Z)$
Guest (pers. com.)	
(*const)	$SW \downarrow = S_0 0.673 \cos(Z)$
Moritz (1978)	$SW \downarrow = S_0 (0.47 \cos(Z) + 0.47 \cos(Z)^2)$
Guest(pers. com.)(e)	
	$SW \downarrow = S_0 (29.35 \times 10^{-3} + 0.347 \cos(Z) + 1.37 \cos(Z)^2 - 22.4 \times 10^{-3} e)$
Guest(pers. com.)(RH)	
	$SW \downarrow = S_0 (0.164 + 0.363 \cos(Z) + 1.28 \cos(Z)^2 - 2.07 \times 10^{-3} RH)$
Guest(pers. com)	
(Quadratic)	$SW \downarrow = S_0 (12.46 \times 10^{-3} + 0.336 \cos(Z) + 1.43 \cos(Z)^2)$
Guest(pers. com.)(RH _i)	
	$SW \downarrow = S_0 (0.458 + 0.399 \cos(Z) + 1.08 \cos(Z)^2 - 4.92 \times 10^{-3} RH_i)$

Table 9. Parametric equations for shortwave radiation under clear skies.

Clear sky downward SW	Mean Error	Standard Deviation	Total Error
Zillman 1972	-0.665	21.716	21.726
Shine 1984	-4.230	23.552	23.929
Bennett 1982	-3.013	25.384	25.562
Guest (pers. com.) (*constant)	1.710	27.274	27.327
Moritz 1978	13.797	38.940	41.311
Guest (pers. com.) (e)	-24.106	42.658	48.998
Guest (pers. com.) (RH)	-19.411	46.377	50.275
Guest (pers. com.) (quadratic)	-35.257	61.027	70.479
Guest (pers. com.) (RH _i)	36.498	68.968	78.030

Table 10. Mean Error, Standard Deviation and Total Error between measured longwave radiation and parametric equations for occurrences of clear skies. The three best formulas are in bold.

The three most accurate predictors were Zillman (1972), Shine (1984) and Bennett (1982). Scatter error plots for the three best formulas show very similar patterns, with Zillman's (1972) remaining most linearly about the zero line (Figure 25). Both Shine (1984) and Bennett (1982) begin to have greater magnitude errors, bending away from the zero line, at higher values of $SW\downarrow$ (Figure 25).

This bending away from the zero line may give the impression of a lesser overall accuracy for the equations, however an examination of their 'Total Error' shows that there is less than 4 W/m^2 difference in error between the top three equations. It is only at the extreme values of $SW\downarrow$ during summer that the error begins to be greater (Figure 26).

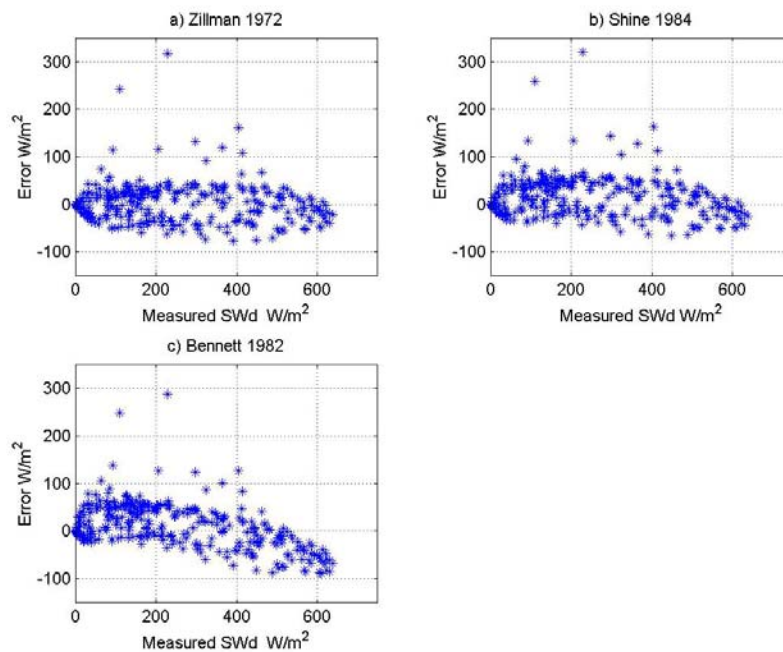


Figure 25. Scatter error plots for the three best $SW\downarrow$ (SWd) parametric formulas under clear skies. Error is calculated from predicted $SW\downarrow$ - measured $SW\downarrow$.

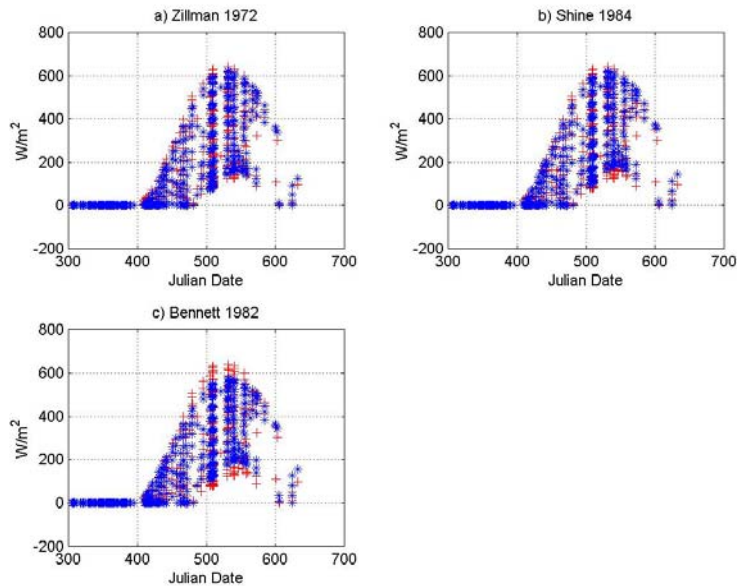


Figure 26. Time series of predicted (blue *) and measured (red +) for the three best parametric formulas under clear skies.

Of the three best predictors, both Zillman (1972) and Shine (1984) required e for the calculations, which significantly complicates the use of these equations without on site measuring instruments. Only Bennett (1982) requires only clear sky condition in order to achieve a predicted value. While the errors increase with increasing SW_{\downarrow} , the overall error is not significantly greater than the other two best predictors, making Bennett's (1982) equation the most desirable for use in prediction models.

Not all of the parametric equations tested were exclusively formulated for Arctic situations, specifically those formulated by Guest (Weddell Sea) and Zillman, which was for general Antarctic applications. Despite this, the performance of Zillman's equation was the best in terms of accuracy.

Plots of the scatter error and time series for all nine parametric equations are located in Appendix A (Figures A19 to A27).

2. Overcast Sky Shortwave Downwelling Radiation

For skies with 100% cloud cover, again using the term overcast, there were only three previously published equations that could be tested (Table 11).

In addition, a simple linear best fit equation was formulated to ascertain if the total error value could be improved upon from the tested equations (Table 12).

Of the three tested equations and one best fit to the data, there was not a large variation in the total error and no significant improvement made by creating a best fit to the data (Table 12). As shown, Guest's (pers. com.) quadratic parametric formula was the best of all predictors by a small margin, even over a linear one fitted precisely to the data. Of interest is that Guest's equation was created using data from the Antarctic (Guest, pers. com.). Guest's formula uses no other measured variable than knowledge that the skies are completely overcast, making it the simplest as well as the most accurate of the formulas. Bennett's (1982) formula, which ranked as the third most accurate of the equations, also required only knowledge of sky condition but was 15 W/m² less accurate for all tested points.

Guest(pers. com.)	
Quadratic	$SW \downarrow = S_0(6.43 \times 10^{-3} + 0.182 \cos(Z) + 0.826 \cos(Z)^2)$
Bryant (linear	
best fit)	$SW \downarrow = S_0(0.4486 \cos(Z))$
Bennett(1982)	$SW \downarrow = S_0(0.346 \cos(Z))$
Guest(pers.com.)	
(*const)	$SW \downarrow = S_0(0.338 \cos(Z))$

Table 11. Parametric equations for shortwave downward radiation under overcast skies.

Overcast Sky downward SW	Mean Error	Standard Deviation	Total Error
Guest (pers. Com.) (Quadratic)	-16.143	55.518	57.817
Bryant (Linear Fit to Data)	-0.004	58.407	58.407
Bennett 1982	24.202	68.835	72.966
Guest (pers.com.) (* constant)	26.089	69.967	74.673

Table 12. Downward shortwave parametric equation error statistics. Bold indicates best performers.

Scatter plots of error and a time series for the formulas for Guest's (pers.com.) quadratic and the best fit created for this data show the variations in the accuracy of the parametric formulas (Figure 27). The best fit for this data set was created using a simple polynomial, which was then reduced to a single constant multiplied by the solar constant modified by the solar zenith angle. While the best fit lost some accuracy in the reduction process, it was reduced in order to be linear like the simplest of the parametric equations.

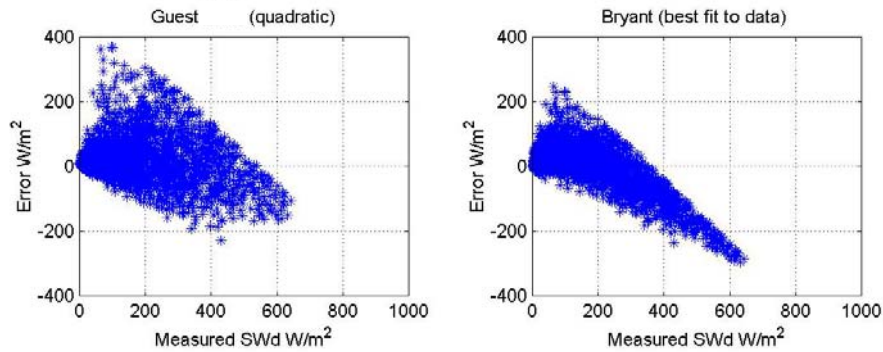


Figure 27. Scatter error plots for best parametric equation and a best fit (linear) for shortwave downward radiation under overcast skies.

A time series of the two best performing equations shows a similar pattern to that observed under clear skies with the greatest error occurring when $SW\downarrow$ (Figure 28). The difference between the linear fit created for this data and the quadratic equation results from Guest (pers.com.) is apparent in the time series (Figure 28).

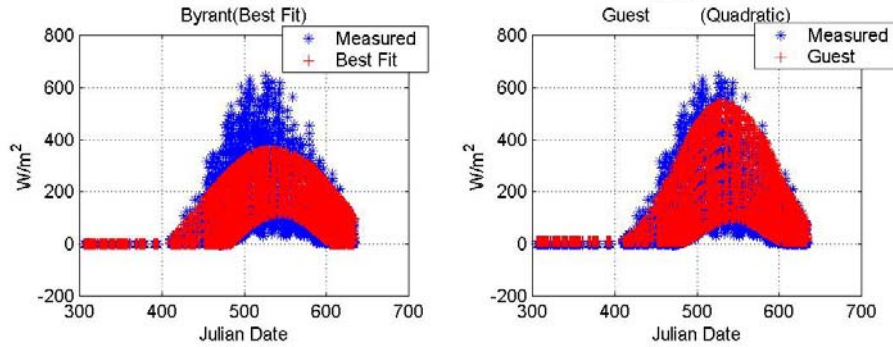


Figure 28. Time series of downward shortwave for the best parametric equation and a linear best fit to the data under overcast skies.

Scatter error plots and time series diagrams for all four parametric equations and the best fit are included in Appendix A (Figures A28-A32).

3. Partly Cloudy Sky Shortwave Downwelling Radiation

For partly cloudy skies in which the hourly averaged cloud fraction ranged from 0.4% to 99.5% there were only two parametric equations that were tested plus a quadratic best fit to these data (Table 13). Error statistics for these equations showed a similar range of error to their longwave counterparts though the overall magnitude of the error was greater (Table 14).

Both of the parametric equations tested required only knowledge of sky condition in addition to sun angle in order to be used. A best fit to the data was created using a polynomial that wasn't reduced to a simple linear multiplier in order to obtain comparative accuracies. Though it was fit precisely to this data set, it didn't perform significantly better than Bennett's (1982) equation (Table 8 & Figure A26). A time series of the two best performing equations depicts a similar pattern to that seen under clear and overcast conditions, with the greatest values of SW_{\downarrow} having the greatest error (Figure A27).

Bryant (Quadratic Best Fit)		$SW \downarrow (\text{partly}) = S_0(0.5795 \cos(Z)^2 + 0.3261 \cos(Z) + 6.5 \times 10^{-4})$
Bennett(1982)		$SW \downarrow (\text{partly}) = S_0 0.72 \cos(Z)(1 - 0.52c)$
Guest(pers. com.) Quadratic		$SW \downarrow (\text{partly}) = S_0(1 - c)SW \downarrow (\text{clear}) + (c)SW \downarrow (\text{overcast})$

Table 13. Parametric equations for shortwave radiation under partly cloudy skies.

Partly Cloudy Sky SWd	Mean Error	Standard Deviation	Total Error
Bryant (Best Fit)	0.000	60.786	60.786
Bennett 1982	17.640	68.906	71.128
Guest (pers.com.) (Quadratic)	-29.458	72.567	78.318

Table 14. Error statistics for parametric shortwave downward radiation equations under partly cloudy skies and a quadratic best fit to the data.

In part, the greater error can be attributed to the wide range of cloud fraction values included under partly skies. In none of the equations is the thickness of clouds or multiple layers accounted for, both of which will affect the amount of downward shortwave radiation significantly.

THIS PAGE INTENTIONALLY LEFT BLANK

IV. CONCLUSIONS

Cloud coverage and base height reflected a distinct U-shaped distribution with a greater percentage of overcast skies than clear, consistent with previously published surveys of cloud coverage in the area (Makshtas et al., 1998). Wintertime cloud coverage shows a more even distribution becoming particularly even during December and January. Overcast percentages gradually increase to a peak in August and September (Figures 5-8).

For each hourly average in which clouds were detected during the hour, the base height of the clouds was less than 1524 meters for most months (Table 2 & Figure 12). In cases in which the cloud bases were low, skies were overcast (9 tenths or greater coverage) 78% of the time, with fewer cases of low clouds and overcast skies in winter (Figure 11).

Net longwave radiation values were significantly less (i.e. less surface cooling) than recent values for the Weddell Sea (Guest, 1998). The thicker and more constant ice cover in the Arctic, as compared with the subsurface heat sources in the Antarctic and a greater aerosol burden, are possible sources for this difference.

The difference in the performance of equations formulated for the Arctic and the Antarctic was greater during clear skies for both longwave and shortwave downward radiation. Antarctic formulas had better error statistics when skies were completely overcast in parameterizing the downward flux for this Arctic data set.

In consistently under-predicting the downward radiation flux under clear skies for both longwave and shortwave radiation, the expectation is for lower downward radiation values in the Antarctic. Under clear skies, where cloud height is no longer a factor, several explanations have been put forward in recent publications. The presence of a greater concentration of aerosols, blowing particles or snow, or diamond dust in the Arctic may be sources of additional downward radiation.

Fifteen parametric equations were tested for acquiring downward longwave radiation against the SHEBA dataset. Of the fifteen, the three best were formulated for Arctic conditions, but only Maykut & Church's (1973) required no other meteorological variable in the equation except temperature. Given the close range of skill shown in the top three performing equations, Maykut & Church's (1973) equation is the best equation according to this data set.

Eleven equations were tested for completely overcast skies, and five tested for partly cloudy skies. For both of these sky conditions, Maykut & Church's (1973) equation was in the top performers and required no other variables, unlike any other top performing equation. For longwave downward radiation, for any cloud coverage, Maykut & Church's (1973) is recommended as the most accurate and simplest to use.

Shortwave downward radiation parametric equations were tested against the SHEBA data set with nine clear sky, four overcast sky and two partly cloudy formulas. Under clear sky conditions, Bennett (1982) was the only equation in the top three that required no meteorological variables at all other than the cloud fraction, though Zillman (1972) was the best in terms of accuracy. The differences between the skill levels of Zillman (1972) and Bennett (1982) were insignificant so Bennett (1982) is recommended as the best under clear sky conditions.

Under overcast conditions, Guest's (pers. com.) formula performed the best of the four formulas and a simple linear fit to the data didn't perform with any greater accuracy than Guest's (pers. com.) quadratic equation. Bennett (1982) did not perform as well under these conditions as Guest's (pers. com.). Guest's (pers. com.) quadratic formula was formulated for Antarctic conditions.

Under partly cloudy skies only two previously published equations could be tested with the SHEBA data with Bennett (1982) performing the best under these conditions. A quadratic fit to the data was created for reference and it's

performance, though obviously better in mean error, did not have a significantly better total error due to a similarly large standard deviation.

Given that Bennett (1982) performed best under clear and partly cloudy conditions and second best under overcast conditions, and also required no meteorological variables, this one is recommended for use with applications in for all sky conditions in the Arctic. If a choice of equations by cloud coverage is feasible, then Guest's (pers. com.) quadratic is best for use in completely overcast conditions.

THIS PAGE INTENTIONALLY LEFT BLANK

APPENDIX A. GRAPHS OF TESTED EQUATIONS

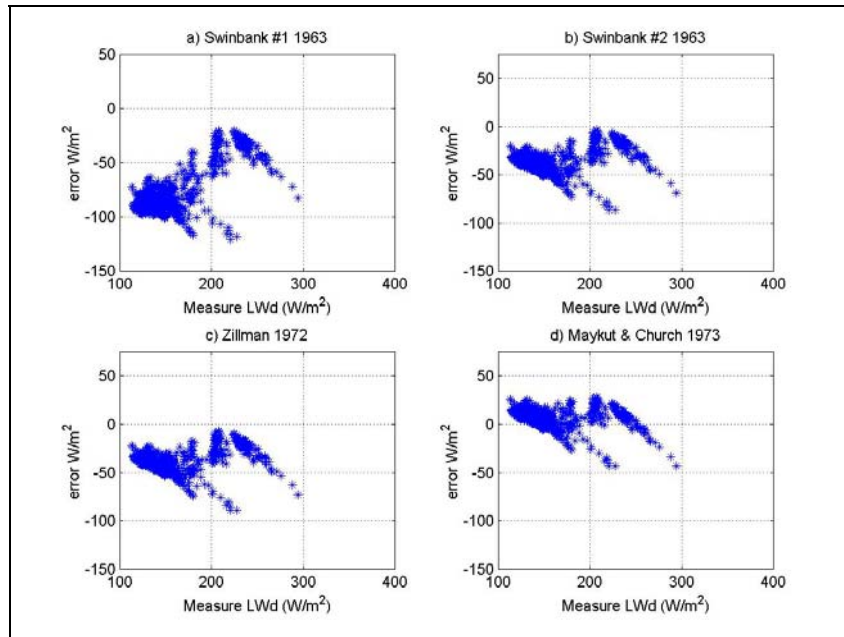


Figure A1. Scatter error diagrams for $LW\downarrow$ under clear skies.

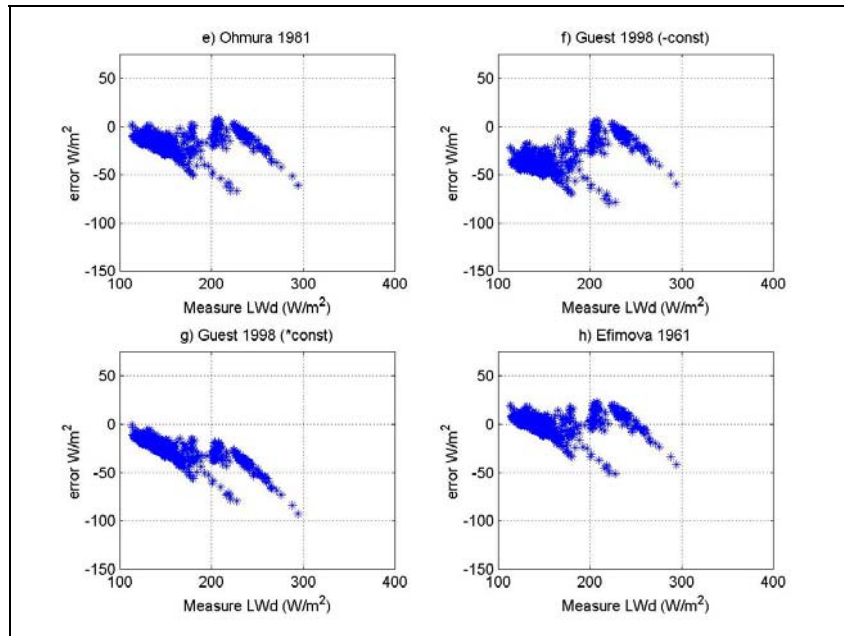


Figure A2. Scatter error diagrams for $LW\downarrow$ under clear skies.

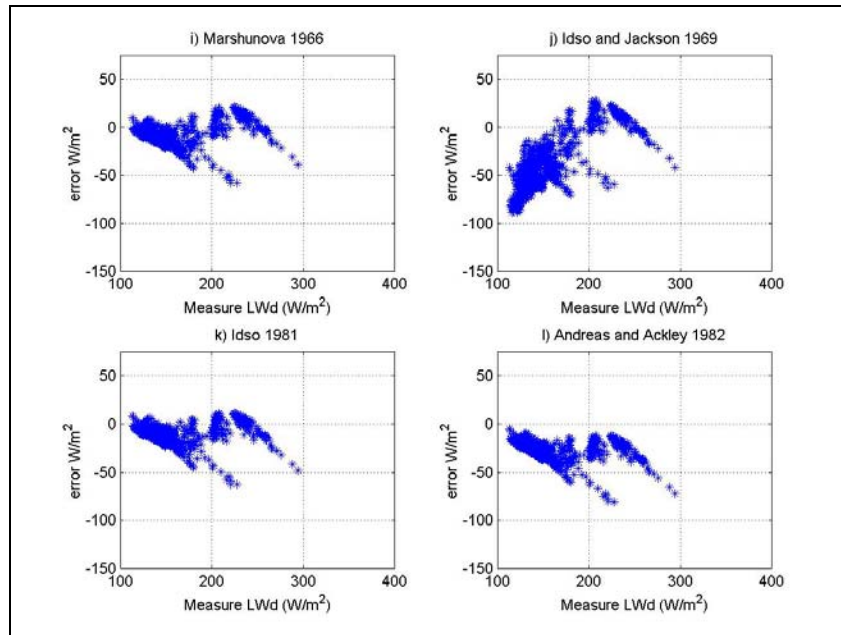


Figure A3. Scatter error diagrams for LW↓ under clear skies.

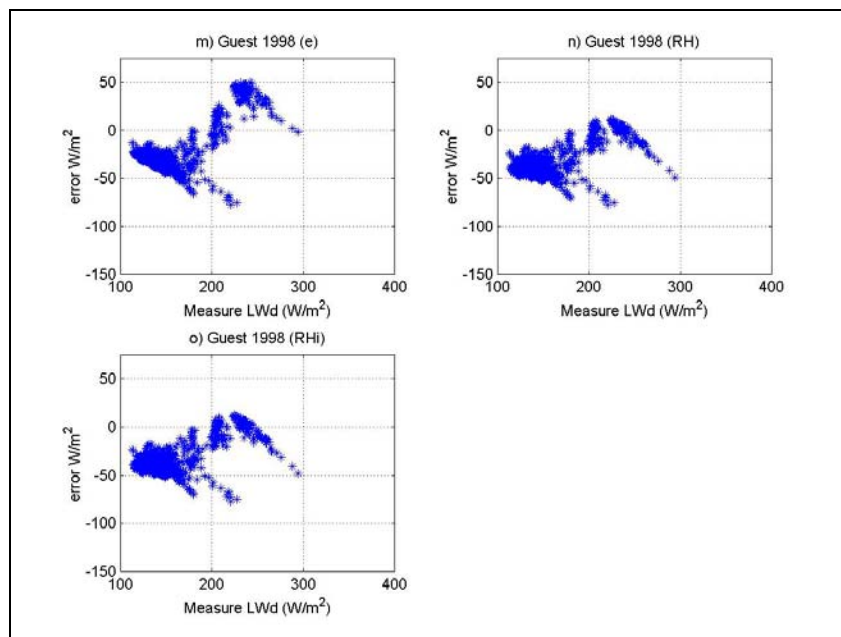


Figure A4. Scatter error diagrams for LW↓ under clear skies.

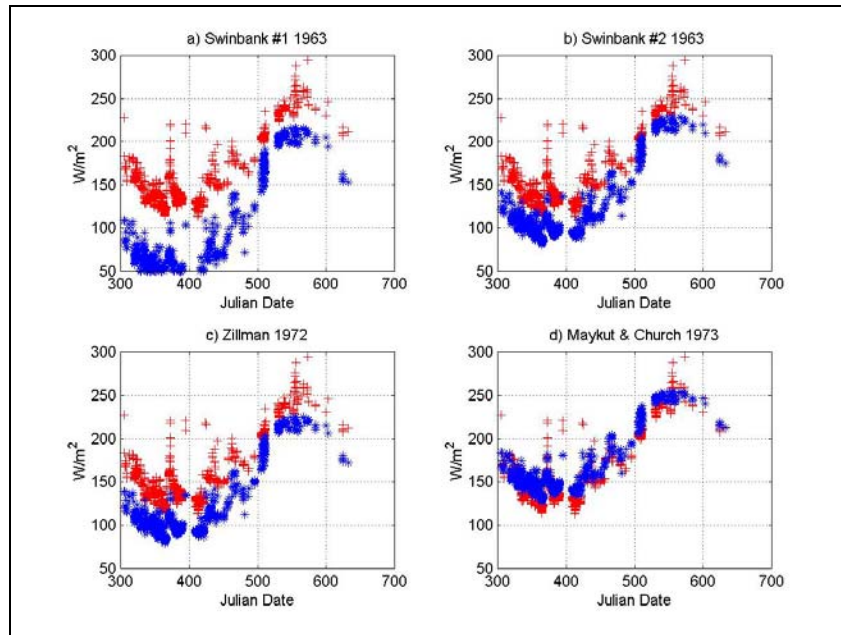


Figure A5. Time series diagrams for $LW\downarrow$ under clear skies. Red + show measured $LW\downarrow$, blue * depict results of parametric equation.

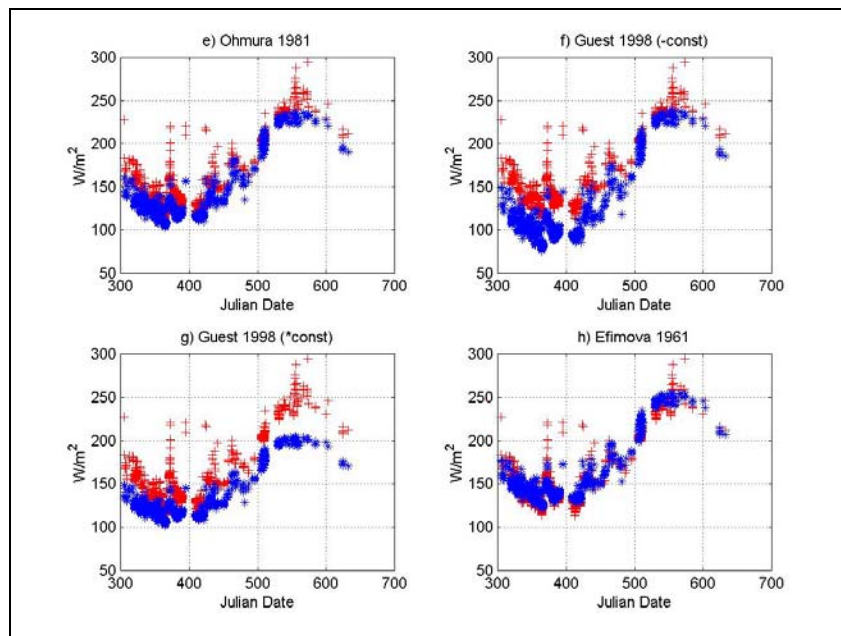


Figure A6. Time series diagrams for $LW\downarrow$ under clear skies. Red + show measured $LW\downarrow$, blue * depict results of parametric equation.

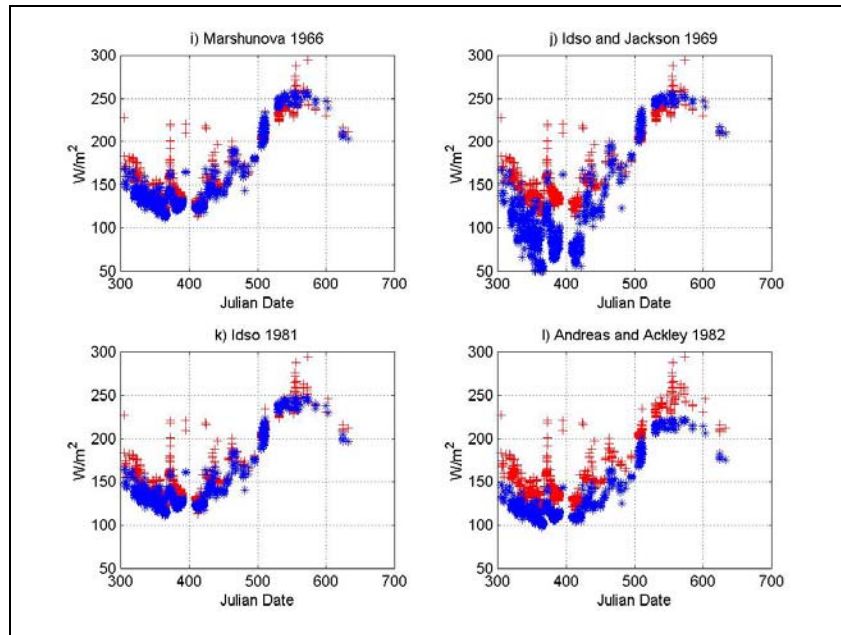


Figure A7. Time series diagrams for $LW\downarrow$ under clear skies. Red + show measured $LW\downarrow$, blue * depict results of parametric equation.

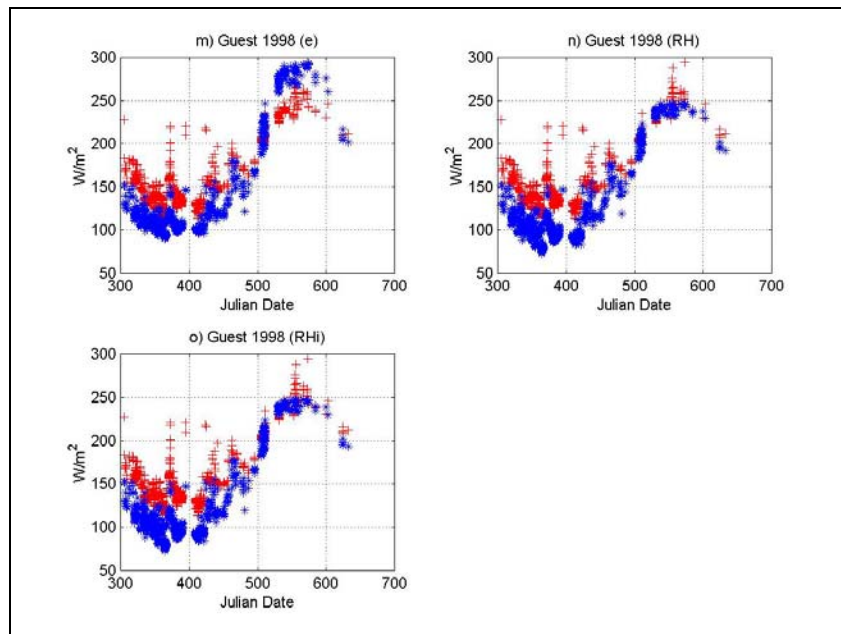


Figure A8. Time series diagrams for $LW\downarrow$ under clear skies. Red + show measured $LW\downarrow$, blue * depict results of parametric equation.

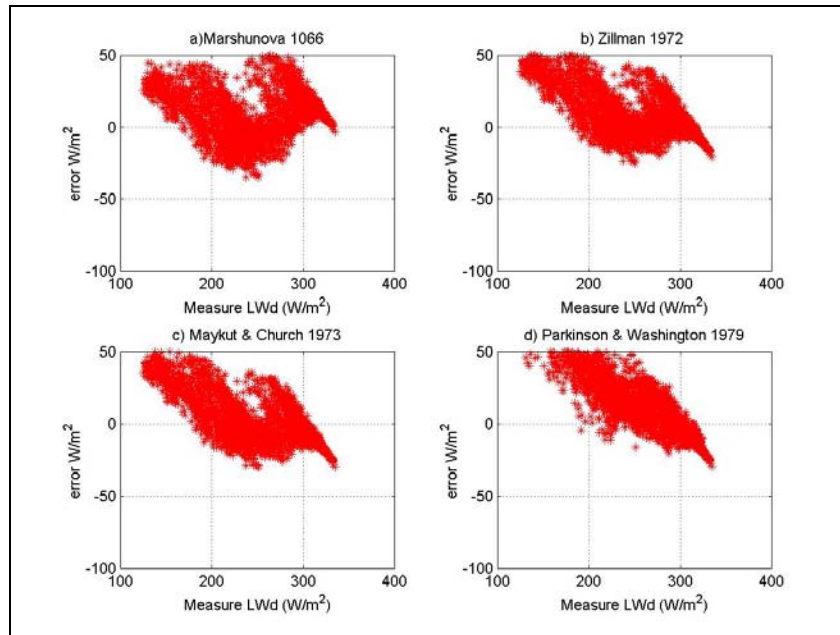


Figure A9. Scatter error diagrams for LW↓ under overcast skies.

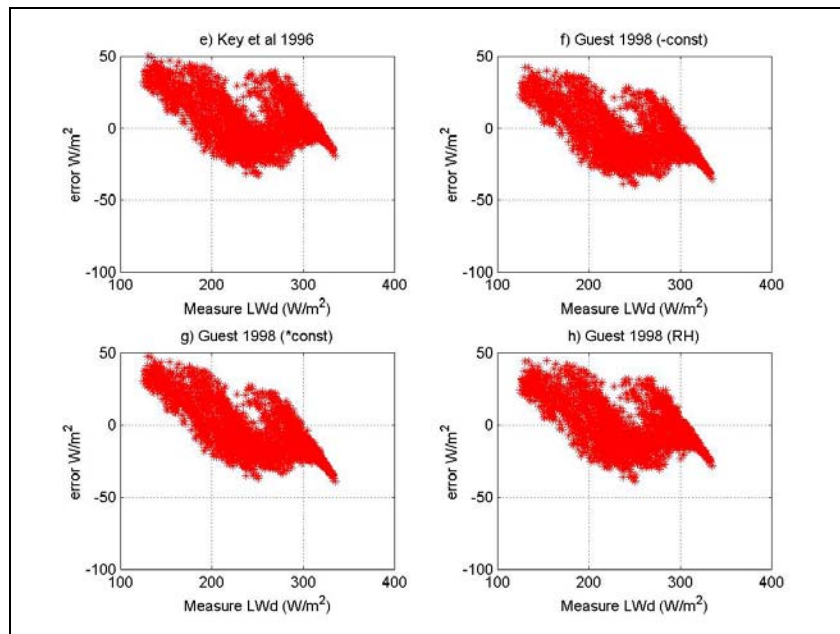


Figure A10. Scatter error diagrams for LW↓ under overcast skies.

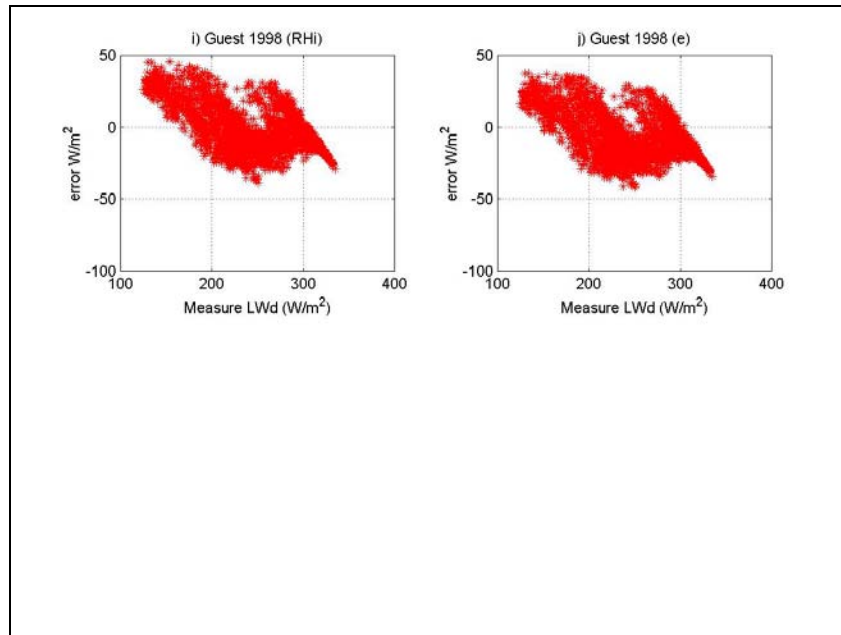


Figure A11. Scatter error diagrams for LW↓ under overcast skies.

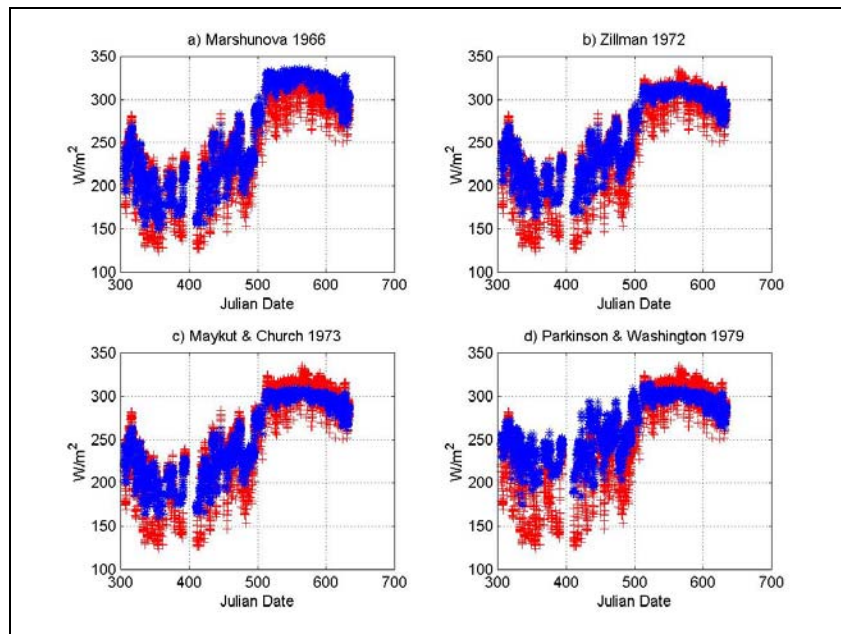


Figure A12. Time series diagrams for LW↓ under overcast skies. Red + show measured LW↓, blue * depict results of parametric equation.

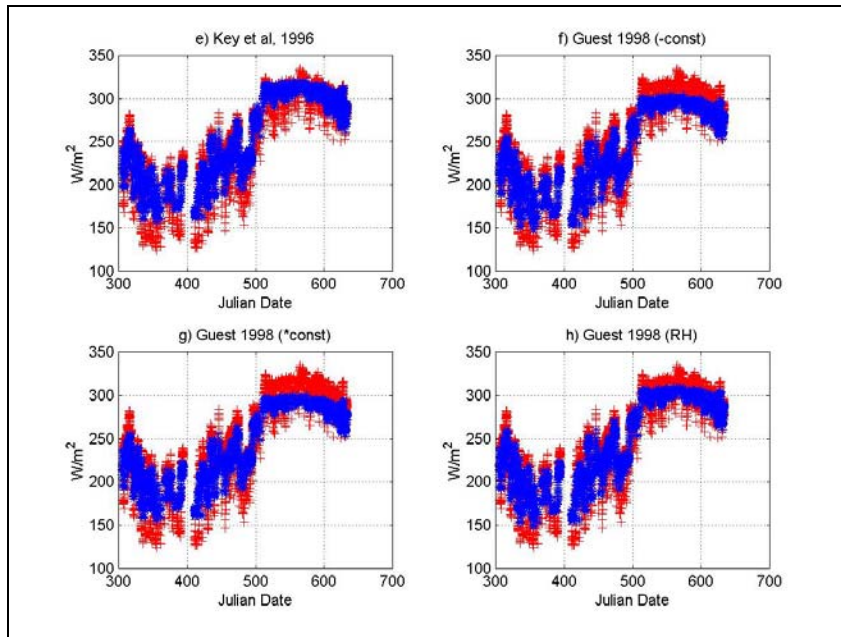


Figure A13. Time series diagrams for $LW\downarrow$ under overcast skies. Red + show measured $LW\downarrow$, blue * depict results of parametric equation.

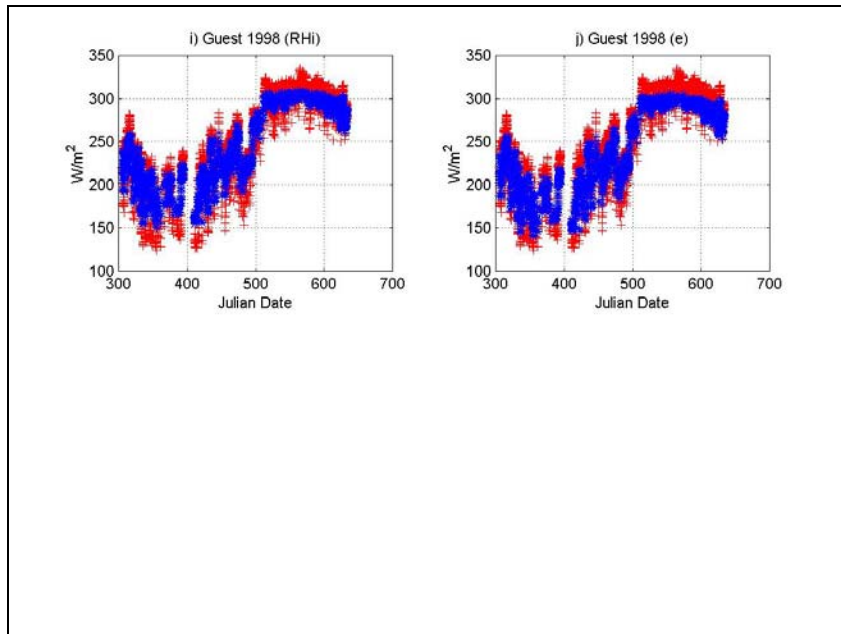


Figure A14. Time series diagrams for $LW\downarrow$ under overcast skies. Red + show measured $LW\downarrow$, blue * depict results of parametric equation.

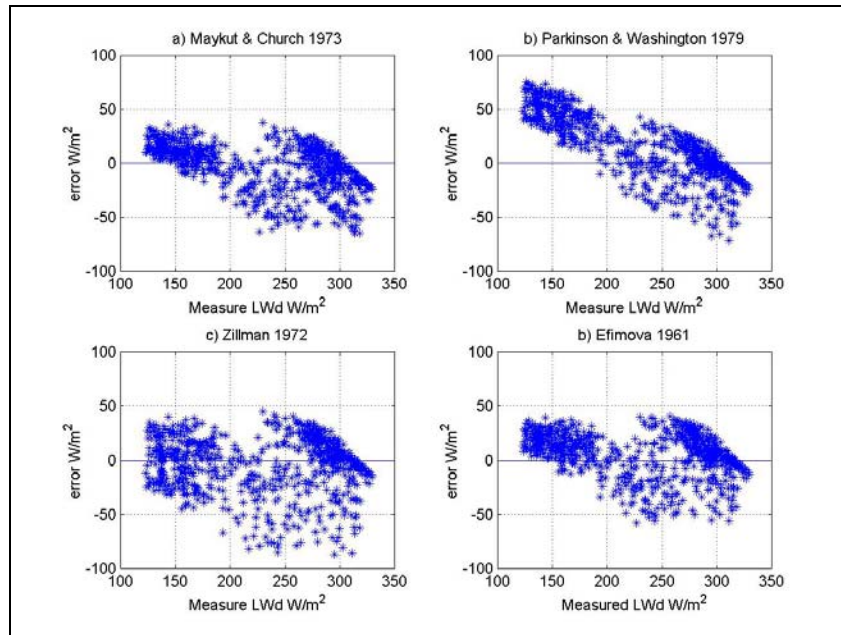


Figure A15. Scatter error diagrams for LW↓ under partly cloudy skies.

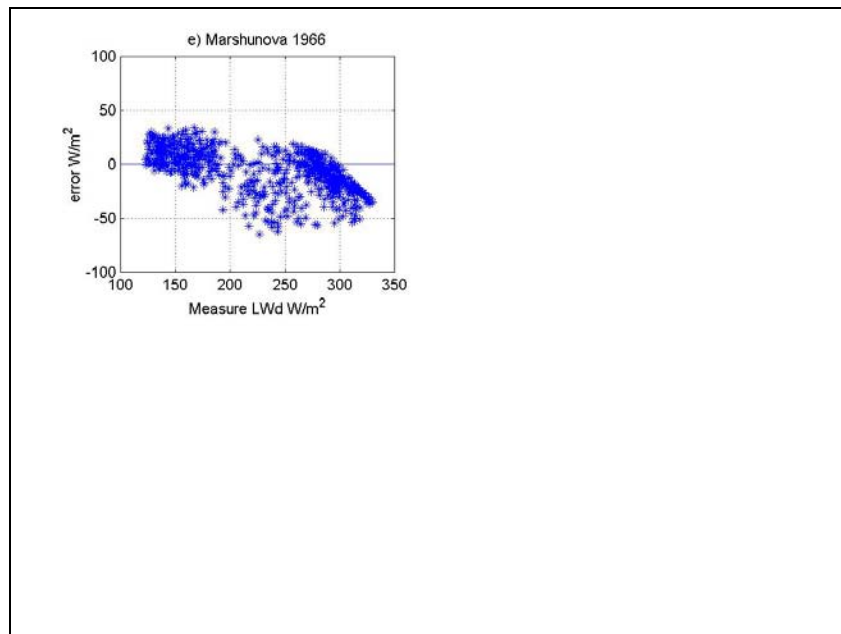


Figure A16. Scatter error diagrams for LW↓ under partly cloudy skies.

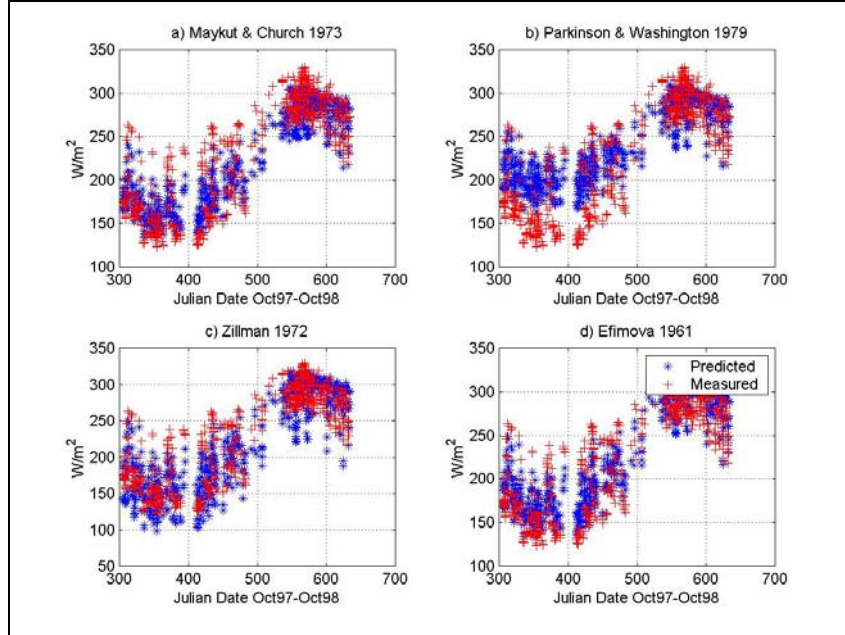


Figure A17. Time series diagrams for LW↓ under partly cloudy skies. Red + show measured LW↓, blue * depict results of parametric equation.

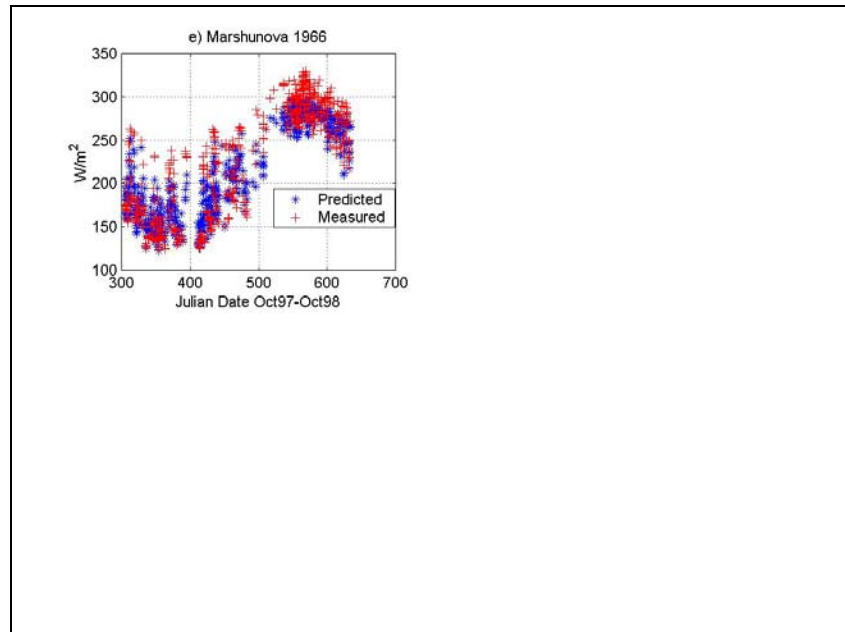


Figure A18. Time series diagrams for LW↓ under partly cloudy skies. Red + show measured LW↓, blue * depict results of parametric equation.

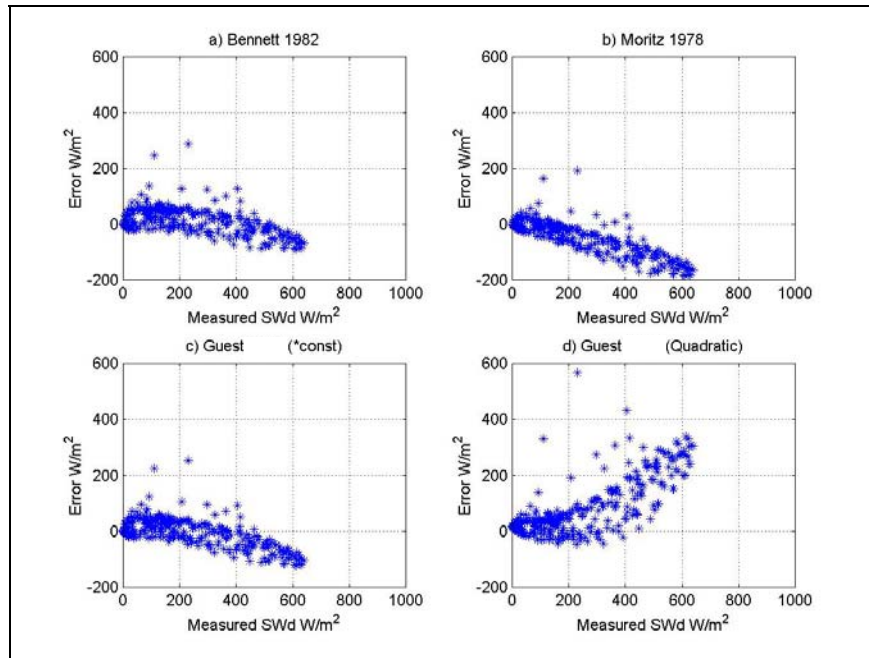


Figure A18. Scatter error diagrams for SW↓ under clear skies.

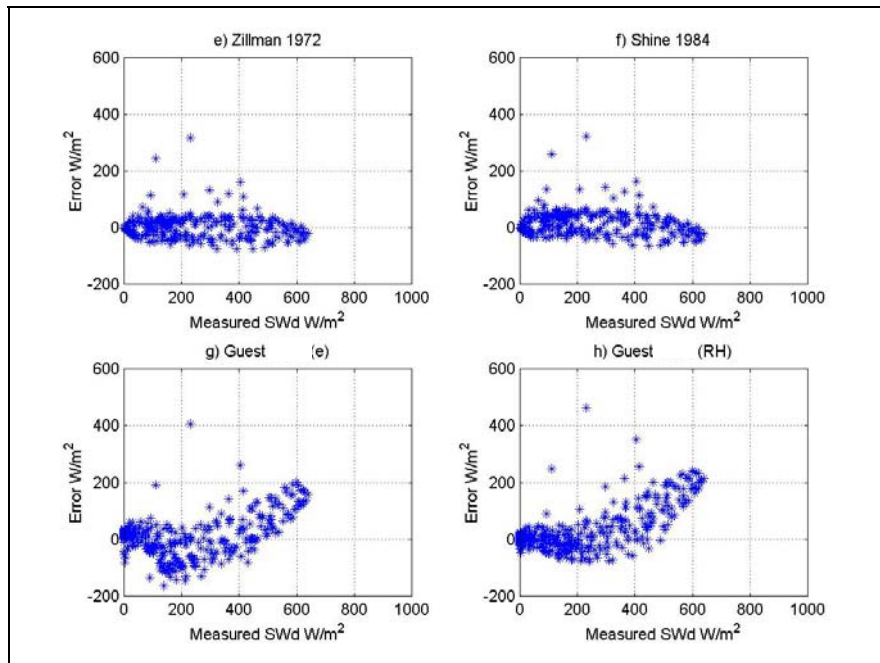


Figure A19. Scatter error diagrams for SW↓ under clear skies.

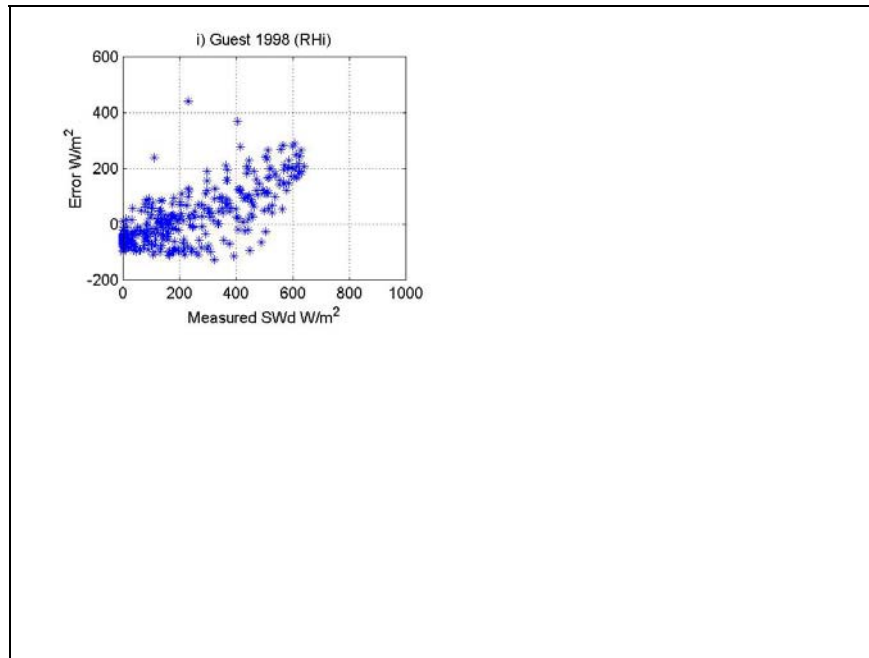


Figure A20. Scatter error diagrams for SW↓ under clear skies.

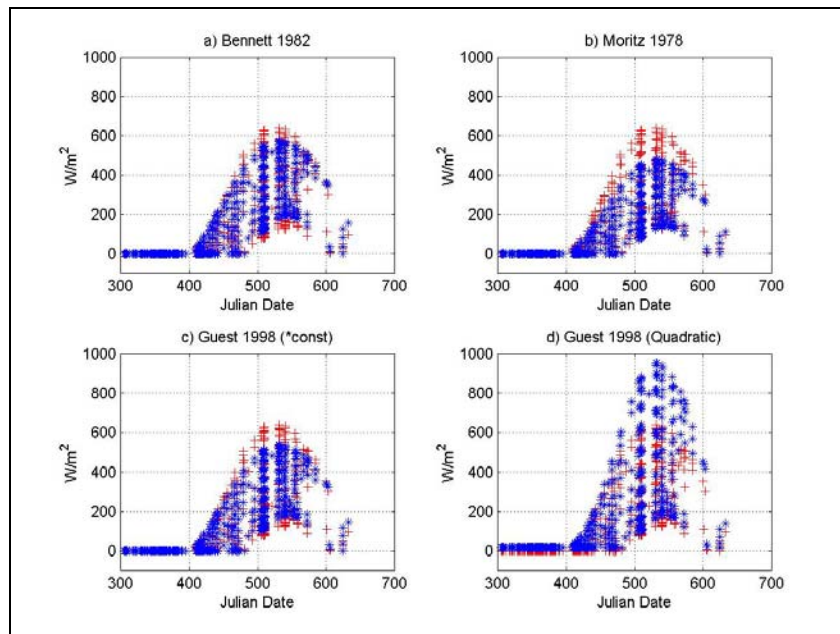


Figure A21. Time series diagrams for SW↓ under clear skies. Red + show measured SW↓, blue * depict results of parametric equation.

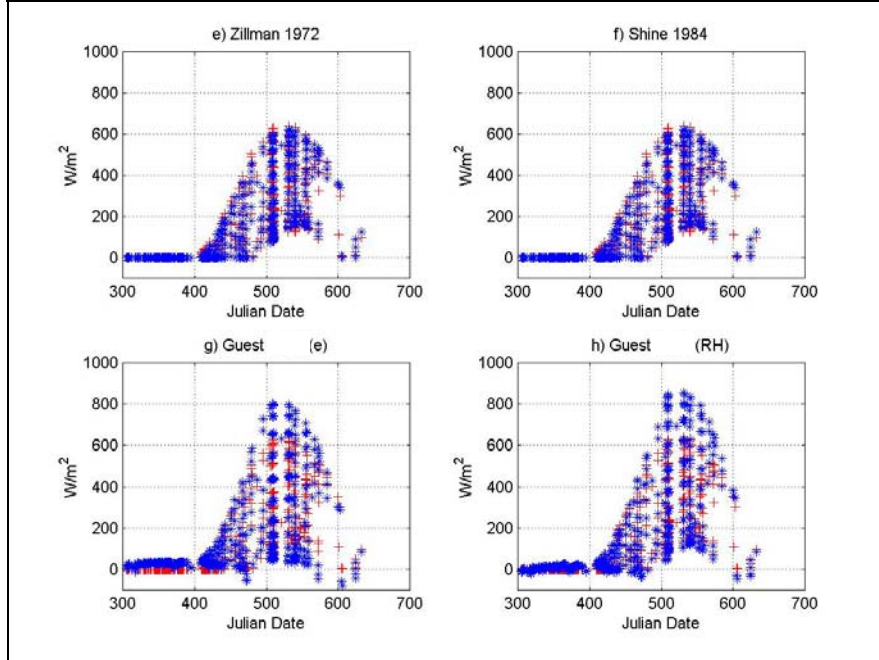


Figure A22. Time series diagrams for SW↓ under clear skies. Red + show measured SW↓, blue * depict results of parametric equation.

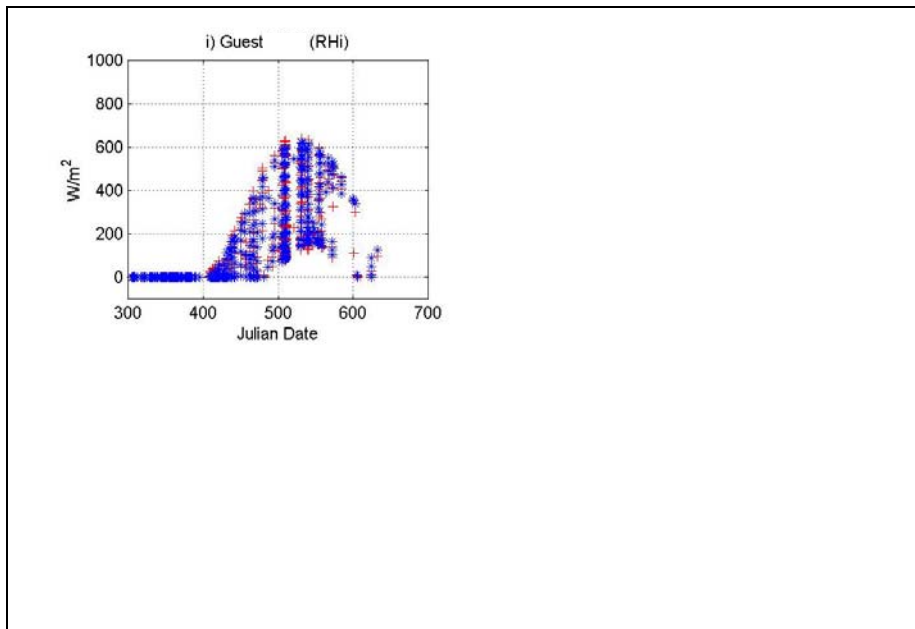


Figure A23. Time series diagrams for SW↓ under clear skies. Red + show measured SW↓, blue * depict results of parametric equation.

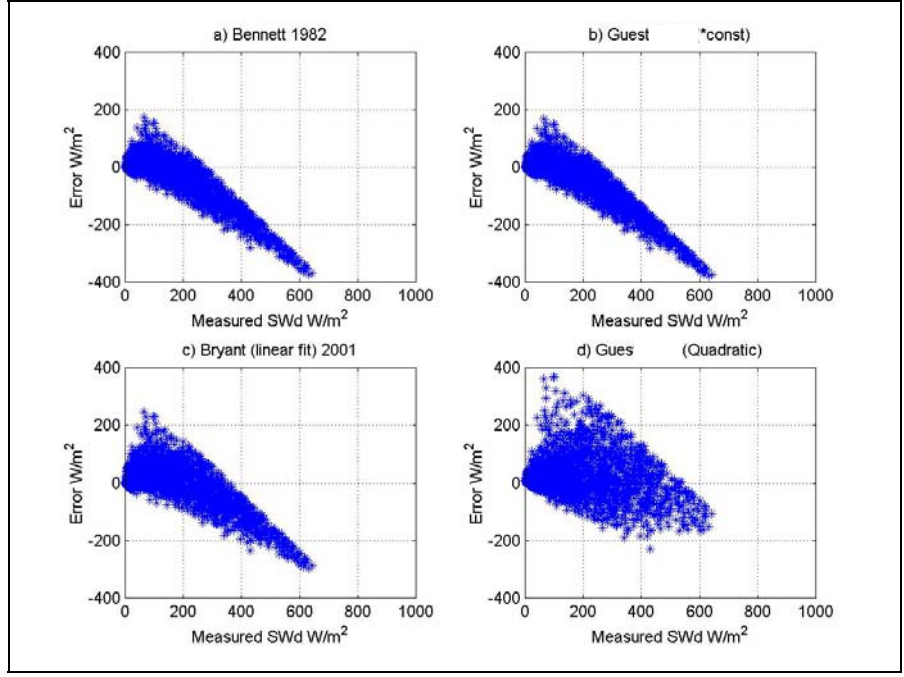


Figure A24. Scatter error diagrams for SW↓ under overcast skies.

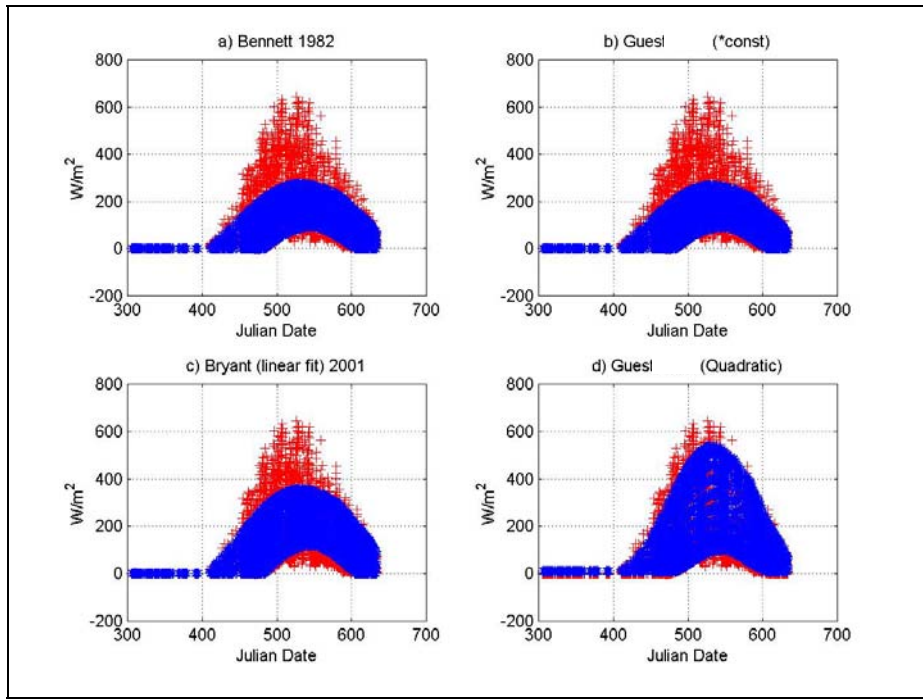


Figure A25. Time series diagrams for SW↓ under overcast skies. Red + show measured SW↓, blue * depict results of parametric equation.

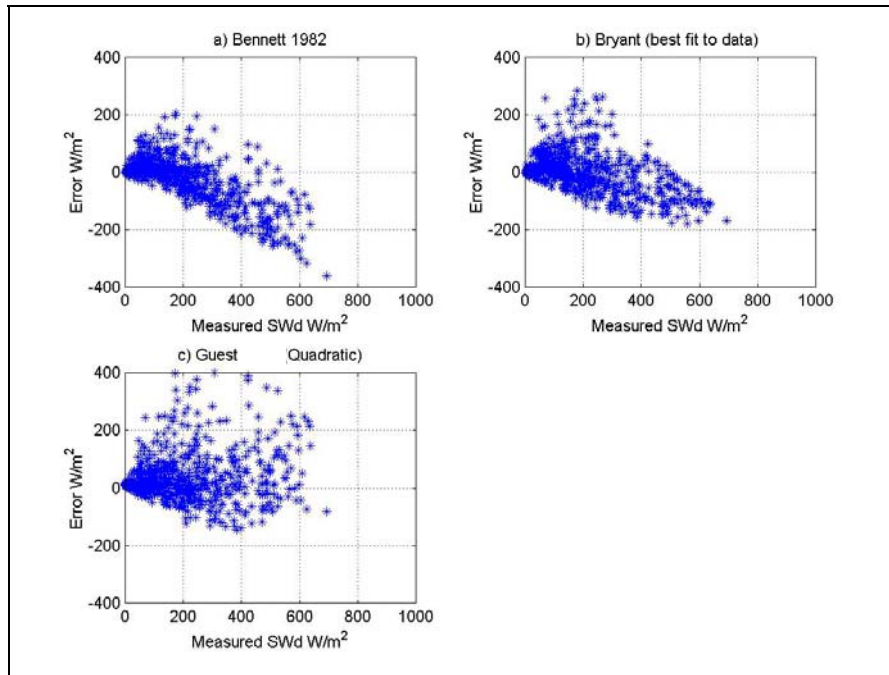


Figure A26. Scatter error diagrams for SW↓ under partly cloudy skies.

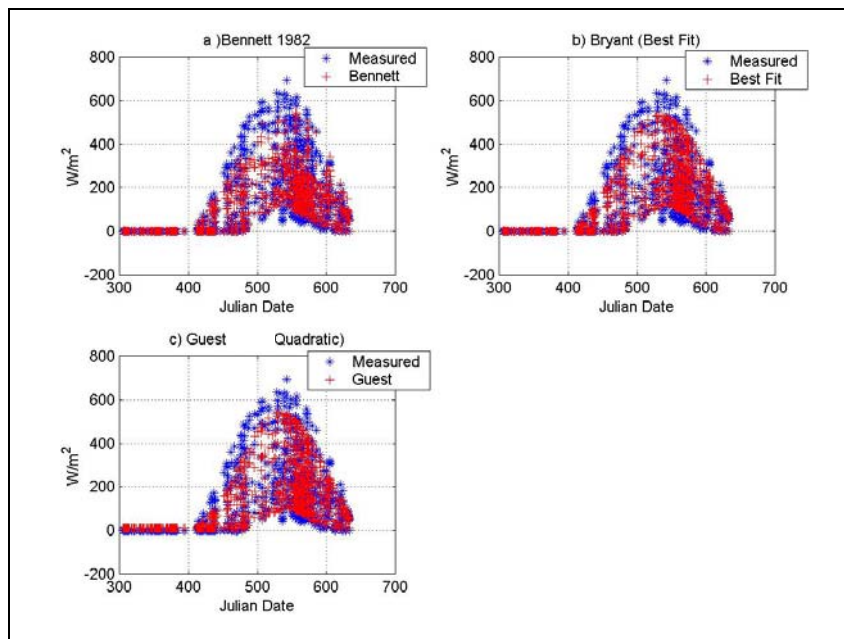


Figure A27. Time series diagrams for SW↓ under partly cloudy skies. Red + show measured SW↓, blue * depict results of parametric equation.

LIST OF REFERENCES

- Andreas, E.L., and S.F. Ackley, On the difference in ablation seasons of Arctic and Antarctic sea ice, *J. Atmos. Sci.*, 39, 440-447, 1982.
- Bennett, T.J., A coupled atmosphere-sea ice model study of the role of sea ice in climate predictability, *J. Atmos. Sci.*, 39, 1456-1465, 1982.
- Curry, J.A., and E.E. Ebert, Sensitivity of the thickness of Arctic sea ice to the optical properties of clouds, *Annals of Glaciology*, 14, 43-46, 1990.
- Efimova, N. A., On methods of calculating monthly values of net long-wave radiation, *Meteorol. Gidrol.*, 10, 28-33, 1961.
- Garratt, J.R., *The Atmospheric Boundary Layer*, 316 pp., Cambridge University Press, 1992.
- Guest, P.S., Surface longwave radiation conditions in the eastern Weddell Sea during winter, *J. Geophys. Res.*, 103, 30,761-30,772, 1998.
- Guest, P.S., Shortwave radiation parameterizations in Weddell Sea, *Pers. Com.*, 2001.
- Idso, S.B., A set of equation for full spectrum and 8-14 microns and 10.5-12.5 microns thermal radiation from cloudless skies, *Water Resour. Res.*, 17, 295-304, 1981.
- Idso, S.B., and R.D. Jackson, Thermal radiation from the atmosphere, *J. Geophys. Res.*, 74, 5397-5403, 1969.
- Jacobs, J.D., Radiation climate of Broughton Island, energy budget studies in relation to fast ice breakup processes in Davis Strait, edited by R.G. Barry and J.D. Jacobs, *Occas. Pap.*, 26, 105-120, Inst. of Arctic and Alp. Res., Univ. of Colo., Boulder, 1978.
- Key, J.R., R.A. Silcox, and R.S. Stone, Evaluation of surface radiative flux parameterizations for use in sea ice models, *J. Geophys. Res.*, 101, 3839-3849, 1996.
- Makshtas, A.P., E.L. Andreas, P.N. Svyashchennikov and V.F. Timachev, Accounting for clouds in sea ice models, CRREL Report 98-9, US Army Corps of Engineers, 1998.

Marshunova, M.S., Principal characteristics of the radiation balance of the underlying surface and of the atmosphere in the Arctic, edited by J.O. Fletcher et al., *Soviet Data on the Arctic Heat Budget and Its Climate Influence, Rep R.M.* 5003-PR, Rand Corp., Santa Monica, Calif. 1966.

Maykut, G.A. and P.E. Church, Radiation climate of Barrow, Alaska, 1962-66, *J. Appl. Meteorol.*, 12, 620-628, 1973.

Moritz, R.E., A model for estimating global solar radiation, Energy budget studies in relation to fast-ice breakup processes in the Davis Strait, edited by R.G. Barry and J.D. Jacobs, *Occas. Pap. 26*, pp. 121-142, Inst. of Arctic and Alp. Res. Univ. of Colo., Boulder, 1978.

Ohmura, A., climate and energy balance of the Arctic tundra, *Zürcher Geogr. Schr.* 3, 448 pp., Geogr. Inst. Zürich, Switzerland, 1981.

Overland, J.E., and P.S. Guest., the Arctic snow and air temperature budget over sea ice during winter, *J. Geophys. Res.*, 96, 4651-4662, 1991.

Parkinson, C.L., and W.M. Washington, A large-scale model of sea ice, *J. Geophys. Res.*, 84, 311-337, 1979.

Persson, P.O.G., C.W. Fairall, E.L. Andreas, P.S. Guest, and D.K. Perovich, Measurements near the Atmospheric Surface Flux Group tower at SHEBA, Part 1: Site description, data processing, and accuracy estimates, technical report in publication, contact Pquest@nps.navy.mil for copy, 2001.

Shine, K.P., Parameterization of shortwave flux over high albedo surfaces as a function of cloud thickness and surface albedo, *Q. J. R. Meteorol. Soc.*, 110, 747-764, 1984.

Swinbank, W.C., Longwave radiation from clear skies, *Q. J. R. Meteorol. Soc.*, 89, 339-348, 1963.

Zillman, J.W., A study of some aspects of the radiation and heat budgets of the southern hemisphere oceans, *Meteorol. Stud. Rep. 26*, Bur. of Meteorol., Dep. of the Inter., Canberra, A.C.T., 1972.

INITIAL DISTRIBUTION LIST

1. Defense Technical Information Center
8725 John j. Kingman Rd., STE 0944
Ft. Belvoir, Virginia 22060-6218
TR@dtic.mil
2. Dudley Knox Library
Naval Postgraduate School
411 Dyer Rd.
Monterey, California 93943-5101
refdesk@nps.navy.mil
3. Naval Ice Center
Suitland Federal Center
Washington, D.C.
liaison@natice.noaa.gov